On the Geographical Variability of the Upper Level Mean and Eddy Fields in the North Atlantic and North Pacific

W. J. EMERY

Department of Oceanography, University of British Columbia, Vancouver, B.C., Canada V6T 1W5

(Manuscript received 21 May 1982; in final form 8 October 1982)

ABSTRACT

All available historical expendable bathythermograph data are used to compute means and standard deviations in temperature for the upper 500 m in the North Atlantic and North Pacific. To take advantage of marked spatial differences in data coverage a variable grid scheme is employed. Both surface and subsurface annual mean temperature distributions agree well with published maps of these quantities. Climatological mean temperature-salinity and salinity-depth curves are used to infer salinities for the mean temperature profiles in order to compute 0/500 db inferred dynamic height and its standard deviation. These mean curves are also used to compute eddy potential energy at 300 m. The maps of mean annual inferred dynamic height agree well with traditional dynamic height maps and appear similar to the maps of mean temperature at 400 m. The North Atlantic eddy potential energy distribution is similar to an earlier calculation. Maps of the standard deviations in inferred dynamic height also represent the geographical variability in mesoscale activity and compare well with a recent global map of mesoscale variability based on satellite altimetry from SEASAT.

1. Introduction

The realization that much of the ocean is populated by mesoscale eddy circulations has created a need for a description of the geographic distribution of mesoscale eddy energy. In an early effort to fulfill this need Wyrtki *et al.* (1976) utilized the historical file of recorded ship drift, determined by merchant ships. Each drift velocity calculation was made over a 24 h period often covering more than 400 km. While this is somewhat larger than the typical expression of an eddy it is likely that most drift calculations will be influenced by those eddies sampled only in part. Thus the resulting map of eddy kinetic energy (EKE), reproduced here as Fig. 1, can be considered as a smoothed, underestimate of eddy activity. It should be remembered here that this presentation includes both barotropic and baroclinic motions over a wide variety of scales and that the term eddy refers to all deviations from a mean state.

In a complimentary approach to the problem Dantzler (1977) employed all available expendable bathythermograph (XBT) data to study the depth variations, from a mean, of the 15°C isotherm in the North Atlantic. Combining these depth fluctuations with mean profiles of the Brunt-Väisälä frequency (from historical hydrographic data), he produced a map of eddy potential energy (EPE) density. Exhibiting highest energies in the western North Atlantic this map (shown here as Fig. 2) generally agrees with the geographic distribution of EKE in Fig. 1. Dantzler's EPE, however, has a distinct zonal minimum between 20 and 30°N absent in the EKE of Wyrtki *et al.* Also the concentration of energy in the northwest extends eastward to only 50°W in EKE (Fig. 1) while it goes out to 35°W in the map of EPE (Fig. 2).

These discrepancies are easily explained by the fundamental differences in the two calculations. Using XBT data Dantzler's (1977) EPE analysis covers only those fluctuations of a baroclinic nature while the EKE calculation includes all motions. Also the ship-drift data file ends before 1970 while the XBT data were taken mainly between 1966 and 1976. The ship-drift estimates are strongly influenced by wind fluctuations while the XBT calculation is affected by strong seasonal changes in the depth and structure of the mixed layer. In spite of these criticisms, because of their uniqueness, these maps have become the standard references for the geographic distributions of mesoscale activity.

It would be useful if a map of eddy potential energy were available for the North Pacific. The primary purpose of the present study is to provide consistent estimates of mesoscale variability, from the historical XBT file, for both the North Atlantic and the North Pacific. A new approach is taken by applying a variable grid scheme to the computation of mean and

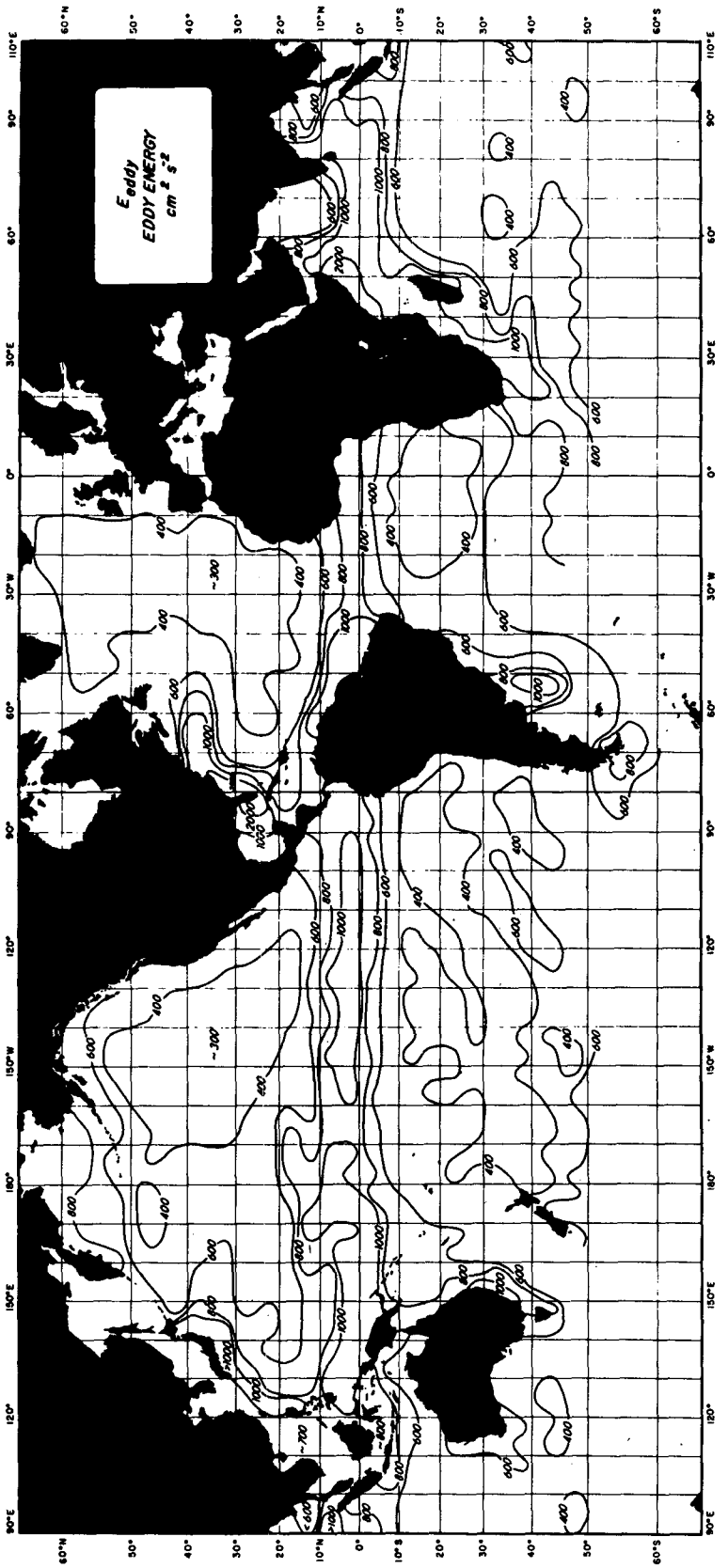

FIG. 1. Eddy kinetic energy ($cm^2\ s^{-2}$) from Wyrtki *et al.* (1976).

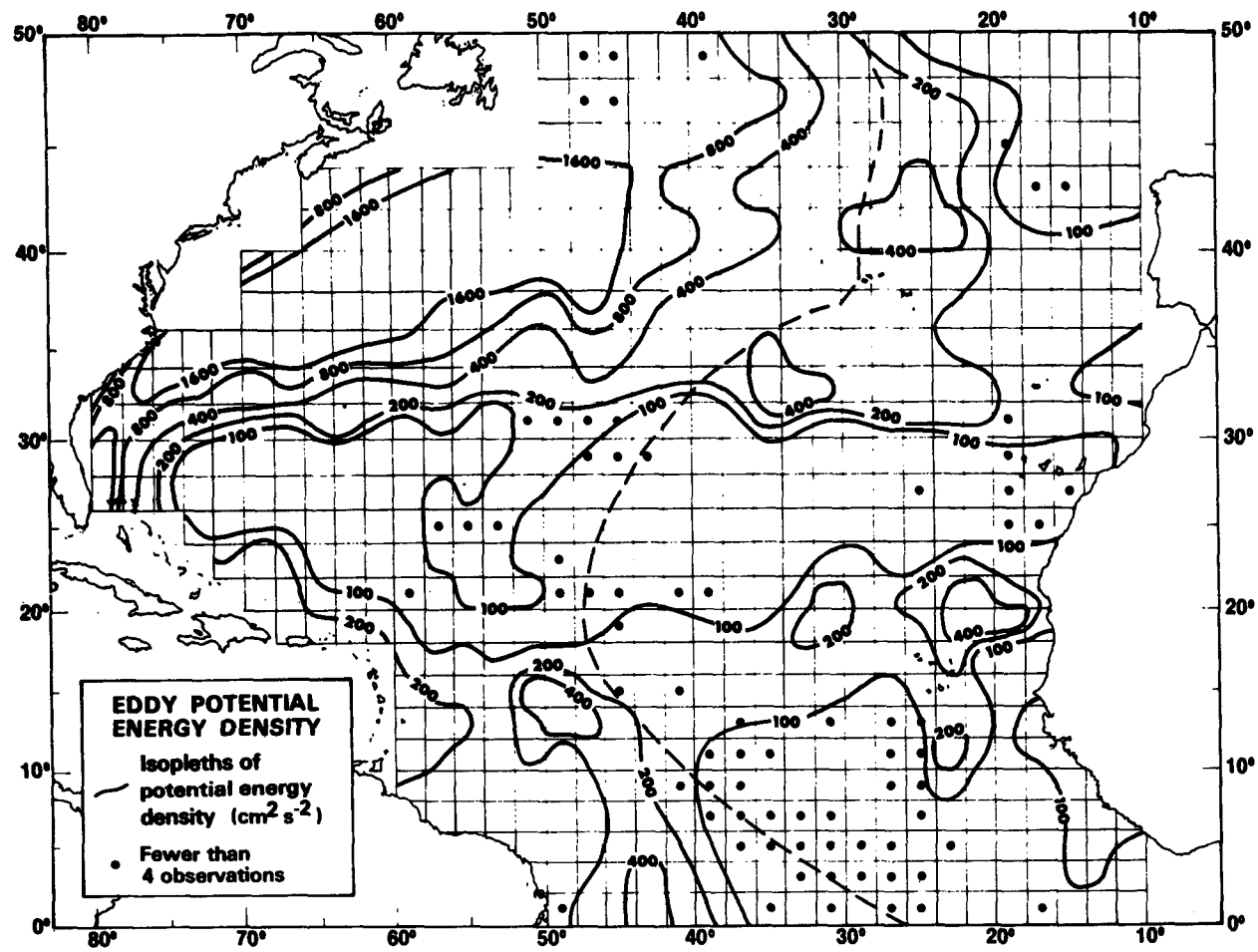

FIG. 2. Eddy potential energy density ($cm^2\ s^{-2}$) from Dantzler (1977).

standard deviation temperature structures, from the XBT file. This scheme takes advantage of regional differences in data coverage providing improved spatial resolution in well sampled areas. To estimate mesoscale energy variability, the XBT profiles are used in conjunction with historical mean temperature-salinity (*TS*) and salinity-depth (*SZ*) curves, computed by Emery and Dewar (1982), to compute the standard deviations of upper layer (0/500 db) inferred dynamic height. Similarly the temperature standard deviations at 300 m are translated into maps of eddy potential energy. These maps of mesoscale eddy activity (both EPE and dynamic height deviations) represent a marked improvement in both the spatial resolution of, and in the amount of, temperature data utilized for this estimation. In addition, the application of inferred dynamic height to this estimation is another demonstration of the utility of a computational technique explored earlier by Emery (1975), Emery and Wert (1976), Emery and O'Brien (1978) and most recently by Emery and Dewar (1982).

As part of this calculation a mean annual XBT temperature climatology is produced and both surface and subsurface (400 m) temperature maps are presented. These fields are found to agree well with previously published temperature maps. The mean XBT temperature profiles are also used to compute maps of mean annual 0/500 db inferred dynamic height which are very similar to published maps of 0/500 db dynamic topography computed from historical hydrographic data. In the following discussion this order is reversed and the variable grid temperature climatology, its computation and its verification are presented first. Subsequent sections deal with the computation and description of mean annual 0/500 db inferred dynamic height and maps of mesoscale variability.

2. Data

Digital XBT data were acquired from the National Oceanographic Data Center (NODC) and from the Naval Fleet Numerical Weather Central (now the

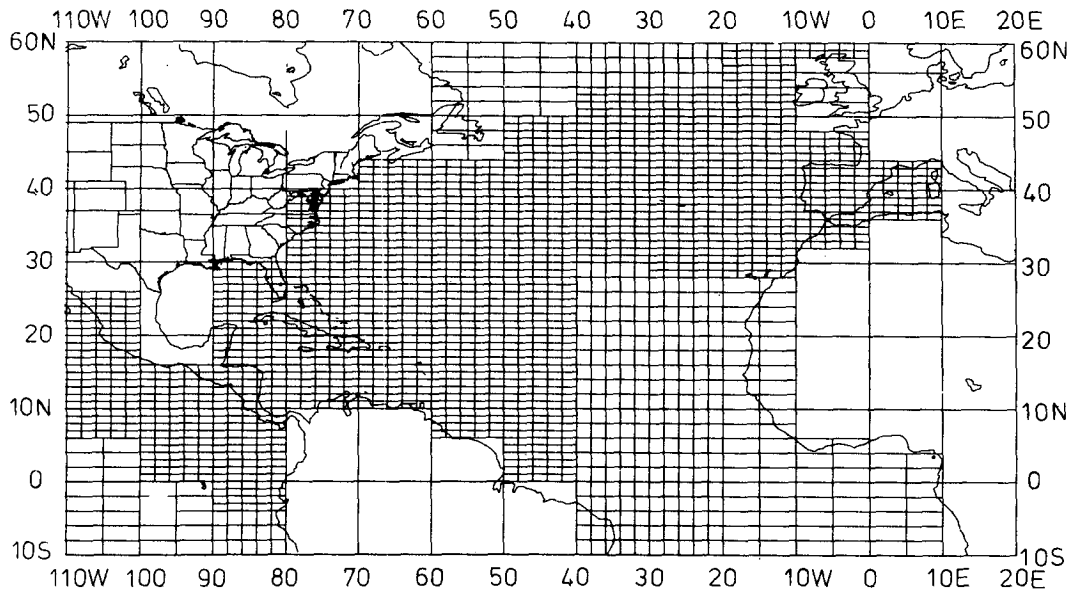

FIG. 3a. Variable grid scheme for the XBT file analysis—North Atlantic.

Fleet Numerical Ocean Center) at Monterey, California. In order to prevent any duplication the files were resorted and compared for identical records. Both files had been updated in 1979 and represented all the data available to the end of that year.

In an effort to edit out drastically erroneous data all extremely shallow (<100 m) XBT casts were eliminated. In addition a preliminary average, over uniform grid squares 2° of latitude by 10° of longitude, was performed to compute mean and standard deviations (σ) over a selection of depths. These depths, which were used for all subsequent analyses, were every 10 m between the surface and 200 m, and every 20 m from 200 to 500 m. Each XBT cast was linearly interpolated to these levels and used to calculate both means and standard deviations. A second pass through the data was then used to eliminate all XBT casts with temperatures lying outside of $\pm 3\sigma$ in any part of the XBT profile. After these editing procedures, which discarded about 25% of the original data, a total of 112 312 XBT casts remained for the North Atlantic and 93 945 for the North Pacific.

A plot of the number of observations per 2° × 10° square revealed the marked non-uniformity in the spatial distribution of XBT casts. A variable grid was employed to improve the resolution in regions where the data were abundant. Efforts to formulate an objective procedure for the selection of this variable grid proved futile and instead the selection was done subjectively. The guiding criterion was to have at least 10 observations per grid unit. Grid sizes ranged from 1° latitude by 2° longitude squares in data-dense regions, to 4° latitude by 5° longitude squares in data-sparse areas. The actual grid system is shown in Fig. 3. The preference of data collection for the coastal regions and the mid-latitudes is readily apparent. Areas of poorest data coverage are the tropical Pacific and the low-latitude eastern North Atlantic. The northernmost-western portions of both oceans also appear to be markedly undersampled.

The distribution of available XBT data is resolved more fully in Fig. 4 where the numbers of observations per grid square are presented. The relative success or failure of the subjective grid selection is readily apparent. Most of the grid points have at least 10 observations while some have considerably more. Some of the 1° × 2° squares do fall below 10 while some of the largest (4° × 5°) squares have enough data to indicate that they likely could be broken down further. Unfortunately, even some of the 4° × 5° squares have less than 10 observations; some as few as 1 or 2. Means and standard deviations were not computed for any grid point with less than 4 observations.

Variations in the number of observations per grid square arose due to the assignment of grid size by area, rather than by individual square. Resulting grid squares with very low data densities should be treated with caution, in the succeeding parameter maps. In the North Atlantic (Fig. 4a) the regions of primary concern are the southeast (10°S–12°N, 0–40°W), the central area (8°N–23°N, 30–50°W), and the northernmost-western (50–60°N, 25–50°W). In the North Pacific (Fig. 4b) much larger areas are poorly covered especially south of 20°N. Areas of lowest data density are the southeast (10°S–10°N, 120–150°W), the southwest (10°S–18°N, 170°W–120°E), and the north central region (40–60°N, 160°W–160°E). Even out-

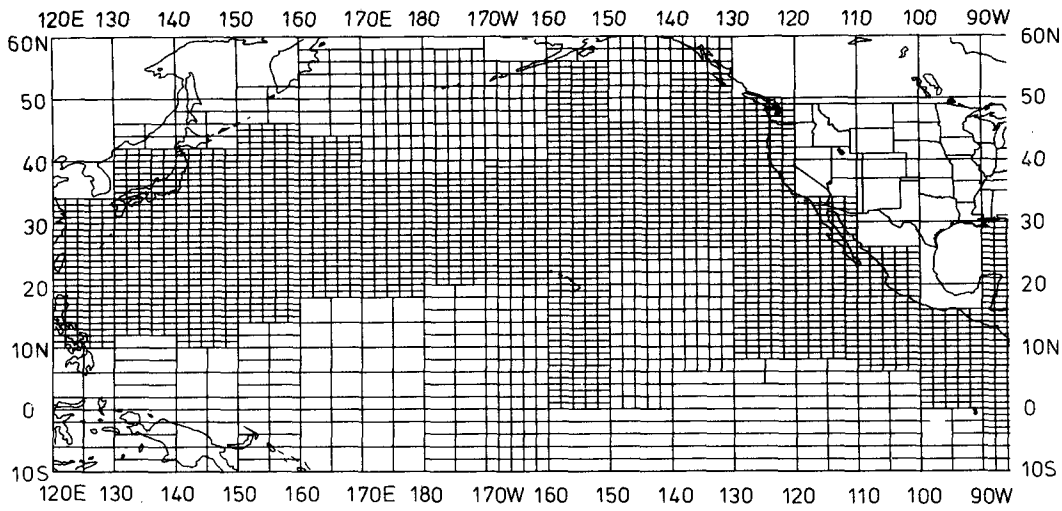

FIG. 3b. Variable grid scheme for the XBT file analysis—North Pacific.

side these areas, however, there are some grid squares with less than 10 observations usually adjacent to squares with many data points. This can be expected to produce some smaller scale structure, in the resultant maps, which will not be related to changes in the parameter being studied. Efforts were made to subjectively smooth some of this noise but much of it still remains. It is hoped that comparisons with existing maps will confirm the validity of the computed distributions.

It is interesting to note that XBT data from major oceanographic programs can be identified in the data coverage maps. The large number of data between Hawaii and California (Fig. 4b) are due to a program sponsored by the U.S. National Marine Fisheries Service (Dorman and Saur, 1978) while the line of data between Hawaii and Adak, Alaska has been maintained by the U.S. Coast Guard. Unfortunately most of the XBT data from the TRANSPAC (White and Bernstein, 1979) program had not yet been added to the NODC file as is obvious from the relative lack of data in the higher latitude central North Pacific. Large numbers of data, near Japan, reflect fisheries activity there along with the terminus of many major shipping routes. The proximity to a major oceanographic institution is also apparently important as the largest number of casts per square is found off of Southern California. This relationship is also evident in the North Atlantic (Fig. 4a) where $1° \times 2°$ grid squares, closest to Woods Hole Oceanographic Institution, exhibit the greatest numbers of data, in excess of 1000 observations per square. In general the number of data per grid point is an order of magnitude greater in the western North Atlantic as compared to the eastern part of this ocean. In the east higher concentrations are found in the mid-latitudes between 30 and 40°N extending eastward into the Mediterranean Sea.

3. Temperature climatology

The editing and averaging procedures, outlined above, produced a climatological temperature structure for the upper 500 m. As a representative sample of the subsurface structure the temperature at 400 m is presented for the North Atlantic in Fig. 5a and for the North Pacific in Fig. 5b. Unfortunately, recent atlases of upper layer temperature structure (Robinson, 1976; Robinson *et al.*, 1979) don't extend down to 400 m making it impossible to compare Figs. 5a and 5b with updated summary maps. It can be said, however, that the general distributions of the temperature contours are consistent with earlier studies. Caution should be exercised in interpreting many of the medium- and small-scale features. The contour lines, originally generated by a computer routine, were subjectively smoothed to reduce small-scale variations. Nevertheless, the remaining fluctuations, especially in the data-poor regions discussed above, are likely not representative of any real variability. As will be shown some of these spatial variations do, however, appear in earlier temperature maps.

For the North Atlantic Fig. 5a can be compared with a similar map produced by Defant (1936) as part of the Meteor reports (shown here as Fig. 6). Although limited to a relatively few hydrographic casts this earlier map agrees fairly well with Fig. 5a. In both, the strong gradient, associated with the Gulf Stream, ranges between 5 and 17°C. The northward inflection of this gradient is located at about 40°N, 45°W in both Fig. 5a and Fig. 6. Both maps also contain a westward tongue of warm water extending along

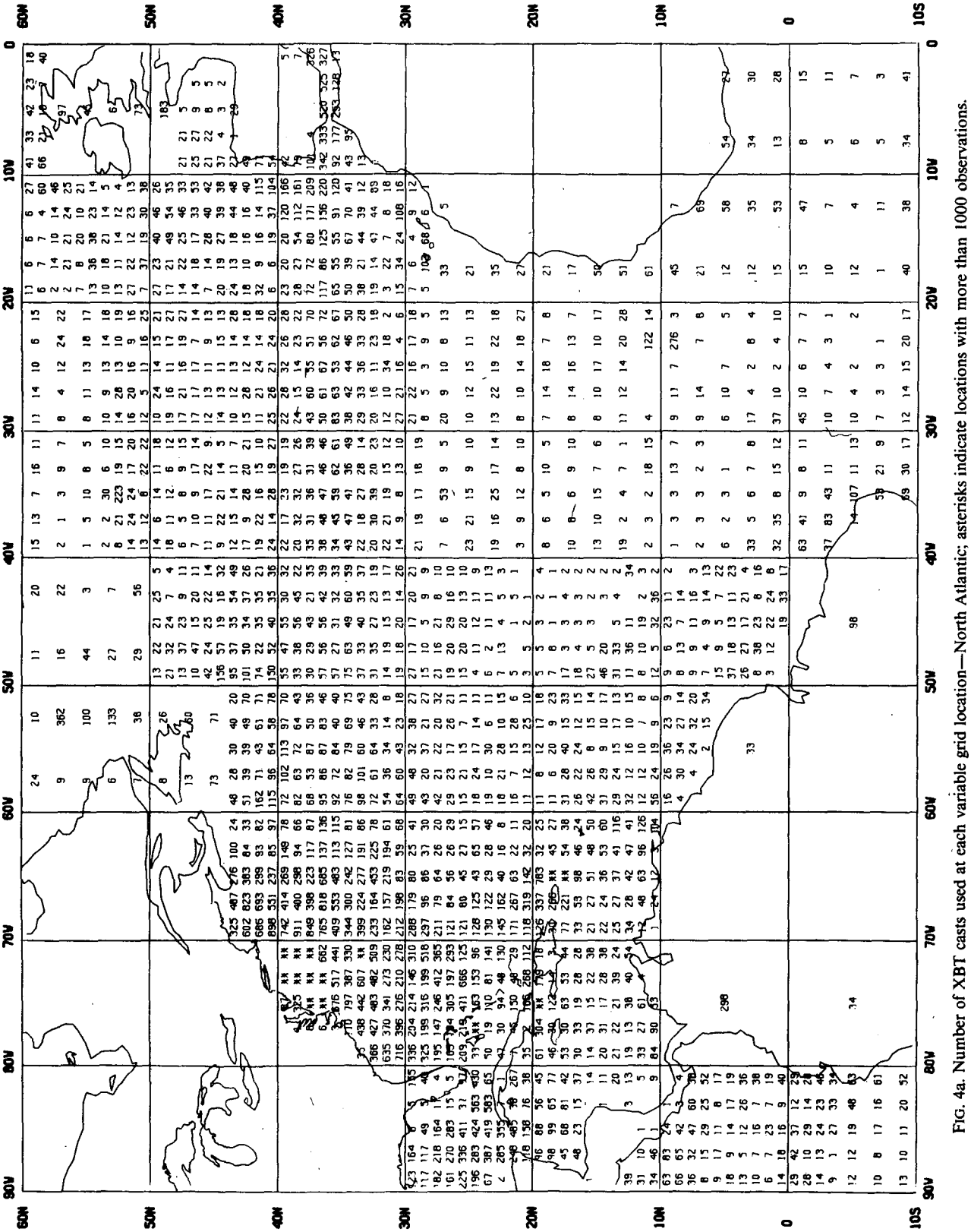

FIG. 4a. Number of XBT casts used at each variable grid location—North Atlantic; asterisks indicate locations with more than 1000 observations.

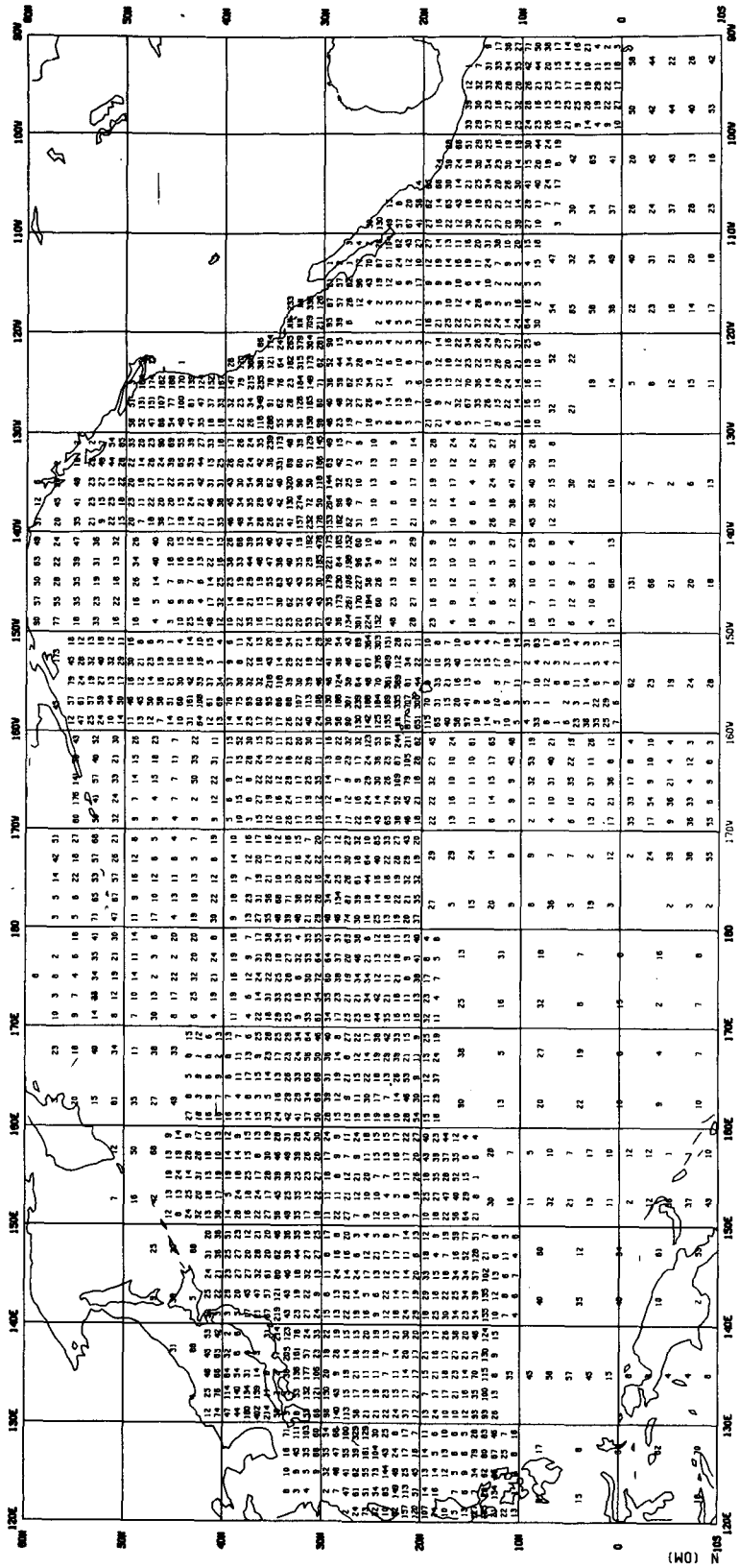

FIG. 4b. Number of XBT casts used at each variable grid location—North Pacific; asterisks indicate locations with more than 1000 observations.

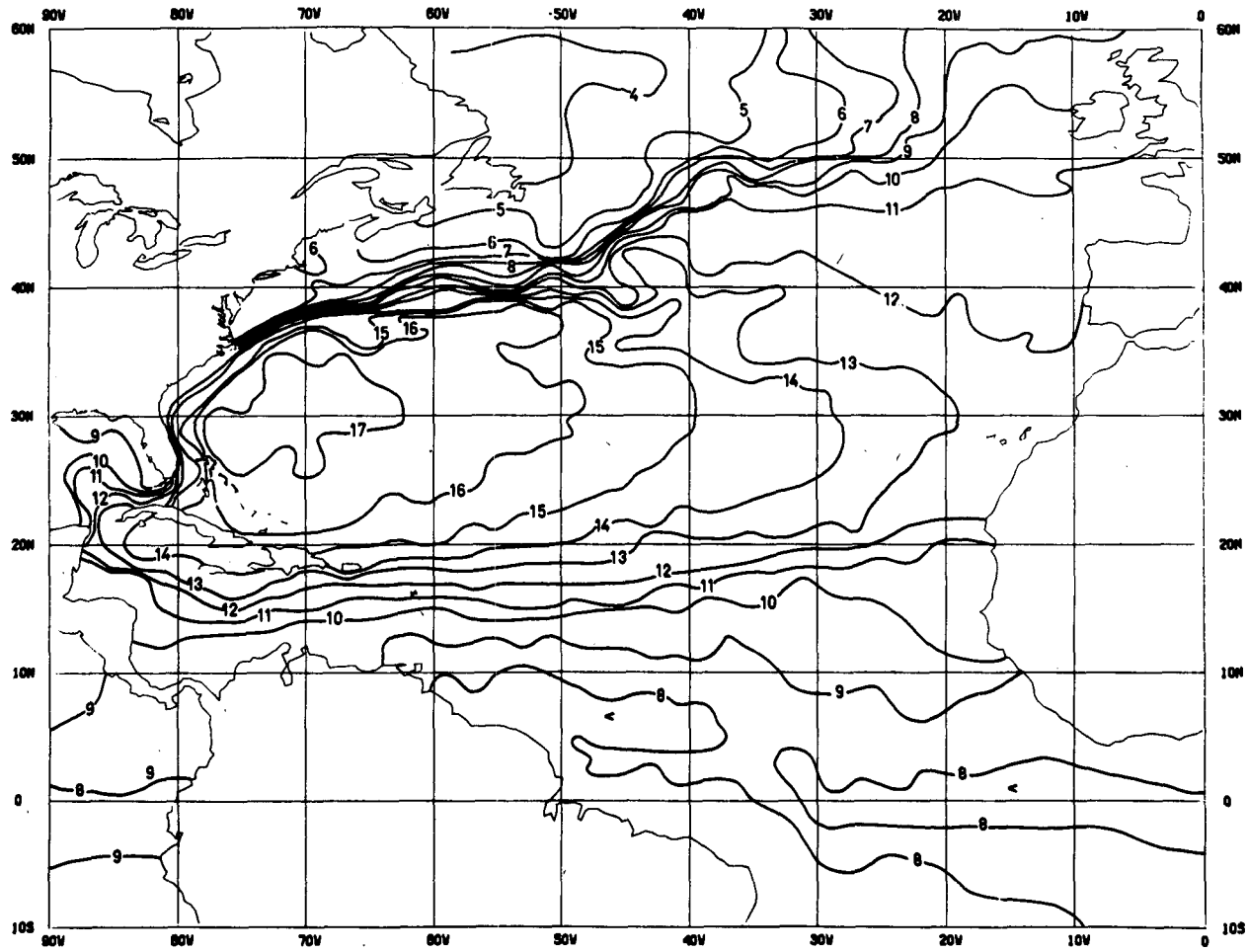

FIG. 5a. Mean annual temperature (°C) at 400 m—North Atlantic.

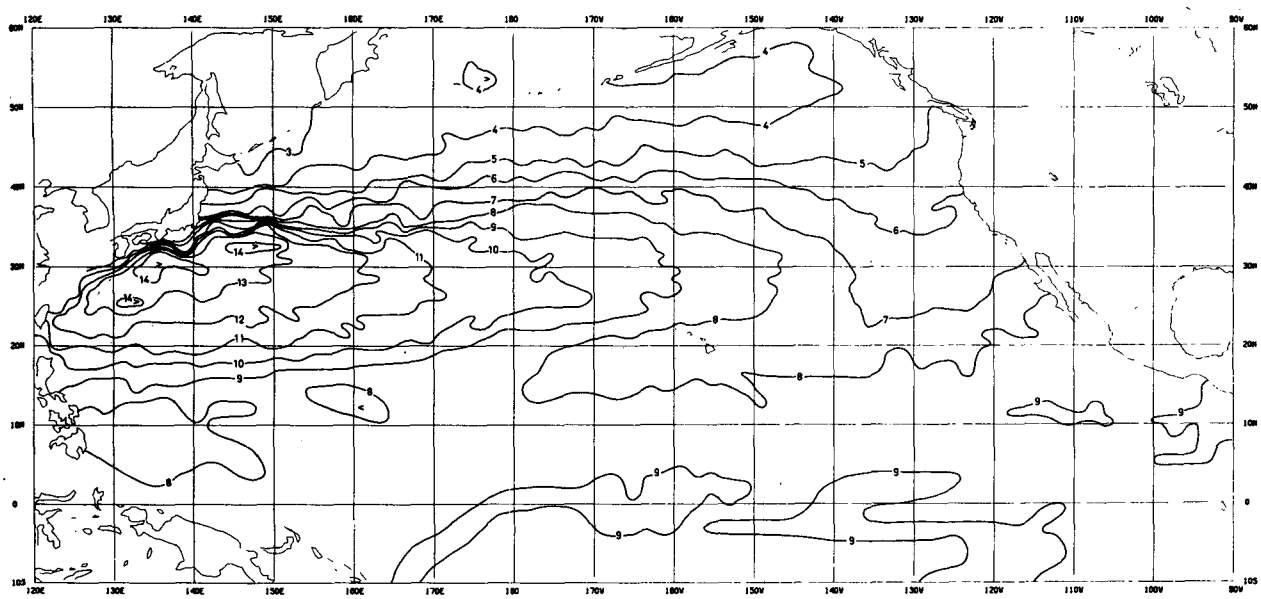

FIG. 5b. Mean annual temperature (°C) at 400 m—North Pacific.

35°N from the Azores (~28°W) to between 50 and 60°W. Between 15 and 20°N a temperature gradient from 10 to 15°C extends east-west across the Atlantic in both 400 m temperature maps. The marked similarities between these 400 m temperature maps, made from very different data sources collected 40 years apart in time, suggest that a stationary, large-scale temperature structure indeed exists.

The temperature at 400 m in the North Pacific (Fig. 5b) is similar to that in the Atlantic except that the gradient associated with the Kuroshio is somewhat weaker than that which follows the Gulf Stream. Also the meanders of the Kuroshio are much less pronounced. Temperature contours in the eastern North Pacific become less indicative of flow as the current turns to cross, rather than parallel, isotherms. Here salinity begins to dominate the upper layer density structure and temperature acts more as a passive indicator of advective processes.

A more comprehensive comparison of the variable grid XBT climatology can be carried out using surface temperature due to the relative abundance of published sea surface temperature climatologies. It should be noted, however, that XBT's frequently record faulty temperatures near the surface as the thermistor equilibrates and the probe starts its descent. Thus comparisons with sea surface temperatures, from XBT profiles, are not always representative of the accuracy over the remainder of the profile. It is, therefore, perhaps best if the annual mean sea surface temperature maps in Figs. 7a and 7b are compared with similar maps, derived from temperature profiles, as presented in Robinson (1976) and Robinson *et al.*, (1979).

The surface temperature map, for the North Atlantic (Fig. 7), contains a lot more structure than was seen in its subsurface counterpart. Some of the increase in spatial variability reflects the stronger surface thermal changes associated with air-sea interaction. Horizontal surface temperature gradients are also stronger than those deeper in the water column as revealed by the packing of isotherms in the western North Atlantic just north of 40°N. Fig. 7a compares well with the annual mean surface temperature presented by Robinson *et al.* (1979; not shown here). The contours in the latter map are somewhat smoother than those in Fig. 7a but both sets of contours exhibit the same general trends. The northward turn of the strong gradient, just north of 40°N, takes place at about 50°W in both maps. Also common to both presentations is a tongue of warm water extending north–northeastward seaward of the strong gradient. Along the eastern boundary both maps express a southward extension of colder water along the coast of southwest Africa consistent with the occurrence of upwelling.

As with the North Atlantic, the North Pacific surface temperature from the variable grid XBT climatology (Fig. 7b) appears much more complex than the corresponding map from the atlas by Robinson (1976). The smoother contours in the atlas surface temperature are due to smoothing procedures not employed in producing Fig. 7b. In spite of the difference in apparent complexity the general trends of both maps agree quite well.

4. Temperature variability

Variability, in terms of temperature standard deviations, was also computed as part of the variable grid climatology. The temperature standard deviation at 400 m was selected as representative of subsurface thermal variability.

For the North Atlantic (Fig. 8a) the 400 m temperature deviation clearly indicates the mesoscale eddy activity associated with the Gulf Stream. As in Dantzler's (1977) eddy potential energy map (herein Fig. 2) highest values are in a tongue stretching eastward from North America, along 40°N, out to between 40 and 50°W. A zonal minimum occupies the latitudes between 20 and 30°N while a narrower zonal minimum crosses the ocean just south of 20°N. Low values are found everywhere along the eastern boundary.

The analogous map for the Pacific (Fig. 8b) also has its highest values in the northwest extending in a tongue eastward from Japan along 35°N. The general level of variability is somewhat lower than in the Atlantic and the maximum tongue is somewhat narrower in the Pacific. Both tongues, however, have similar zonal extents stretching about 30° of longitude out from the western boundary. In the North Atlantic the 2.0°C contour extends from about 75 to 45°W while in the North Pacific the same contour stretches from about 135 to 165°E.

Farther south the zonal minimum and maximum bands are absent in the North Pacific. As a southeastward extension of the strong maximum tongue, a region of somewhat higher values spreads east to about 130°W at 20°N. Small tongues of higher values are also found, at this latitude, protruding westward from the eastern coastal boundary. Values in the south (<10°N) and north (>45°N) appear to be uniformly low. It should be pointed out here that at low latitudes thermal variability is restricted to the very shallow upper layer while in the north salinity variability tends to dominate fluctuations in the density structure. Thus in both of these regions the temperature standard deviation, at 400 m, is unlikely to be representative of mesoscale variability.

5. Inferred dynamic topography

In this section the mean temperature profiles of the variable grid climatology are used in conjunction with

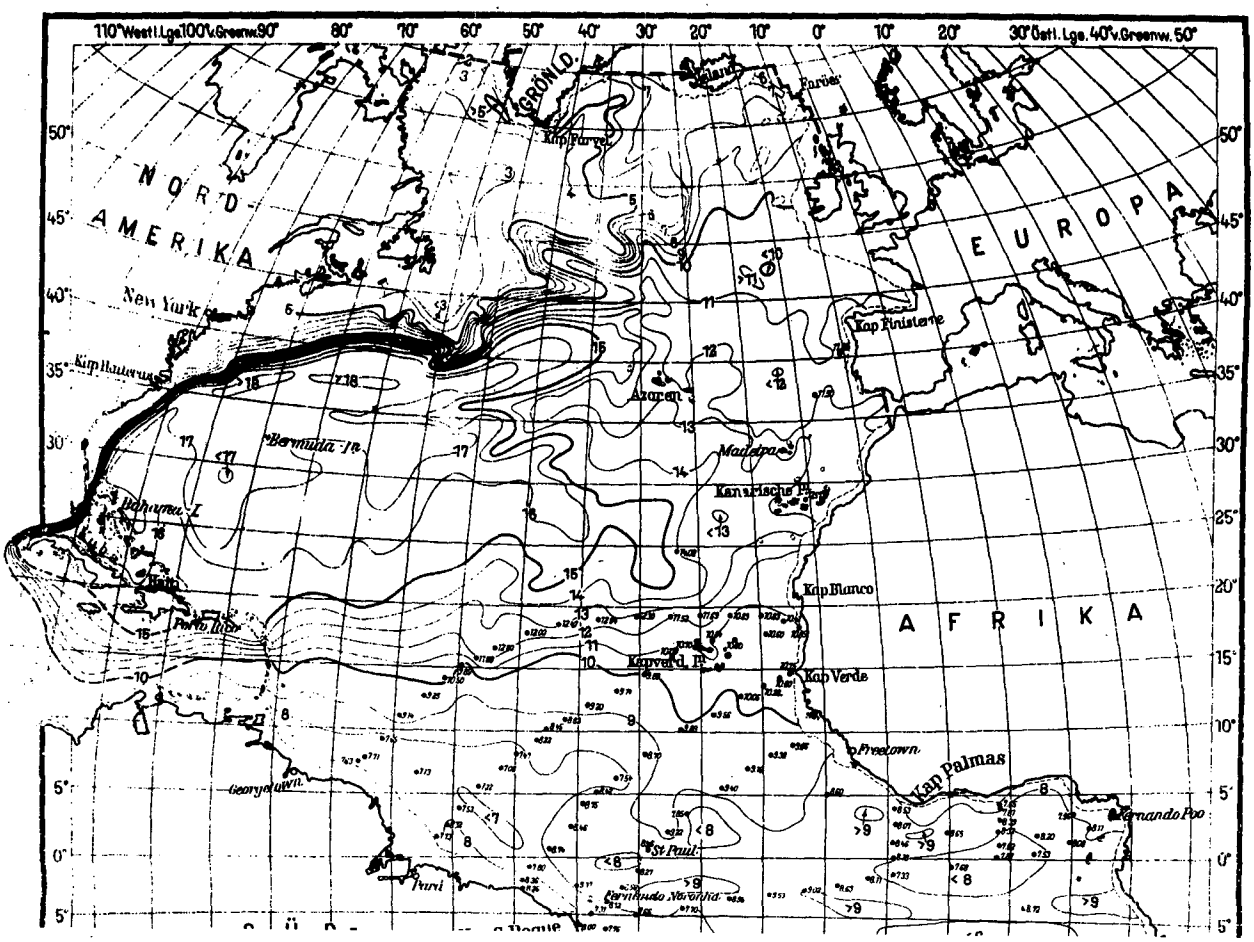

FIG. 6. Temperature at 400 m from the *Meteor* atlas (Defant, 1936).

historical mean curves of temperature versus salinity and salinity versus depth, to produce maps of upper layer (0/500 db) inferred dynamic height. The resulting maps of mean annual inferred dynamic topography are then compared with existing maps of traditional dynamic height computed from hydrographic casts.

In some sense it has become traditional to use well-conserved *TS* curves to provide salinities to match an observed temperature profile. Such a procedure was explored as early as 1947 by Stommel and has seen increased recent use. In a series of papers (Emery, 1975; Emery and Wert, 1976; Emery and O'Brien, 1978) Emery has pursued the application of this technique to the computation of inferred dynamic height in the North Pacific. In the most recent of these studies (Emery and O'Brien, 1978) a problem with using *TS* curves at higher latitudes was specifically addressed. At these latitudes salinity becomes increasingly important in determining the density. Also the frequent occurrence of a subsurface temperature minimum leads to a non-single-valued *TS* curve. As a possible alternative to *TS* curves, for the northern North Pacific (>40°N), Emery and O'Brien (1978) used the mean salinity-depth (*SZ*) relationship. In many parts of this region, away from coastal influences, this procedure appeared to yield reliable inferred dynamic heights.

This conclusion was reviewed in a recent summary analysis of both the North Atlantic and the North Pacific by Emery and Dewar (1982). Using all available hydrographic and CTD data, mean *TS* and *SZ* curves were computed and used to calculate inferred dynamic topography from the hydrographic temperature profiles. Comparisons between these and traditional dynamic heights (computed from observed temperature and salinity) confirmed the recommendation of Emery and O'Brien (1978) that in the higher latitude North Pacific *SZ* inferred dynamic height was more reliable (smaller rms difference with true dynamic height). Thus for the North Pacific a combination of *TS* and *SZ* curves should be used to formulate maps of inferred dynamic topography.

This was not the case for the Atlantic, however,

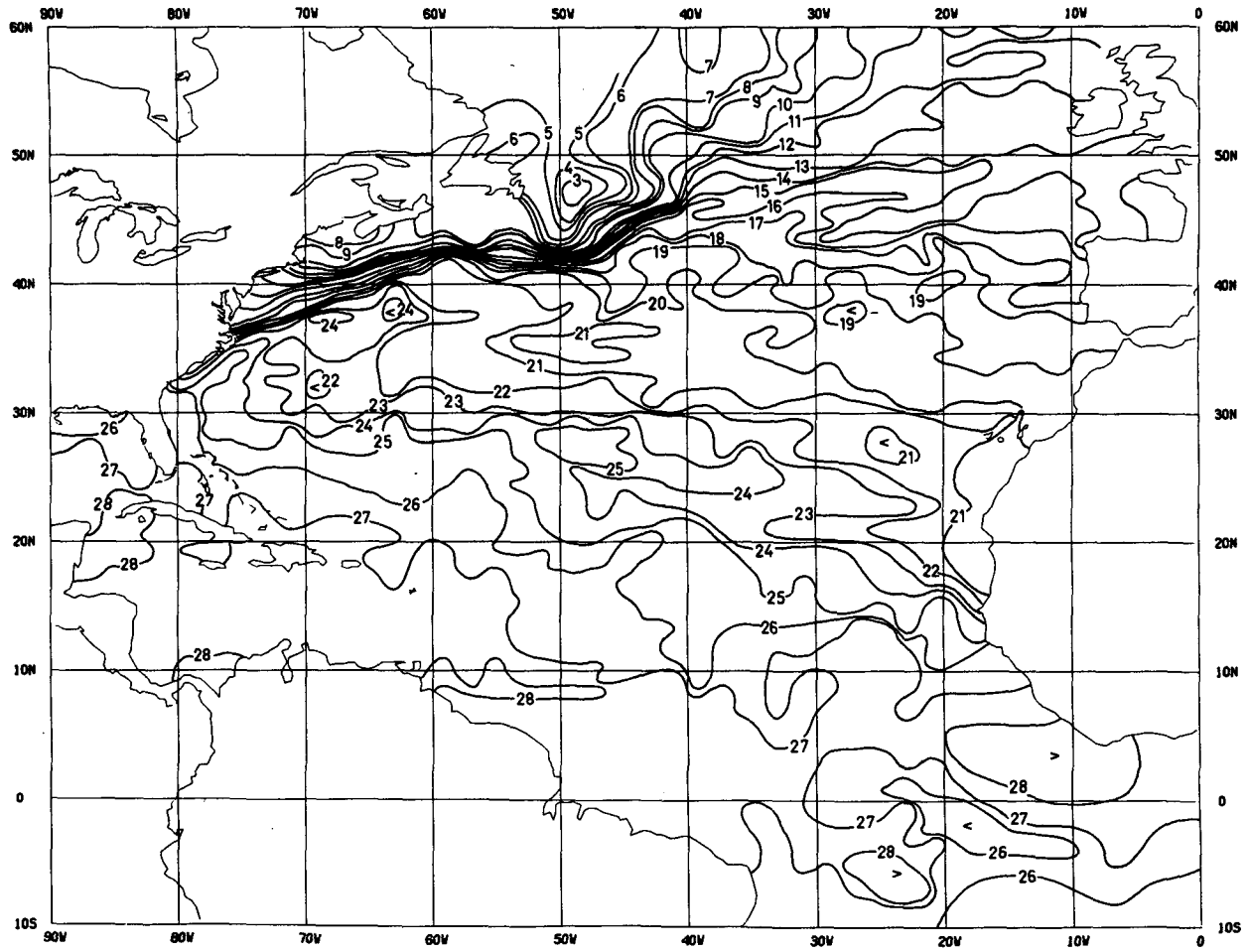

FIG. 7a. Mean annual sea surface temperature (°C)—North Atlantic.

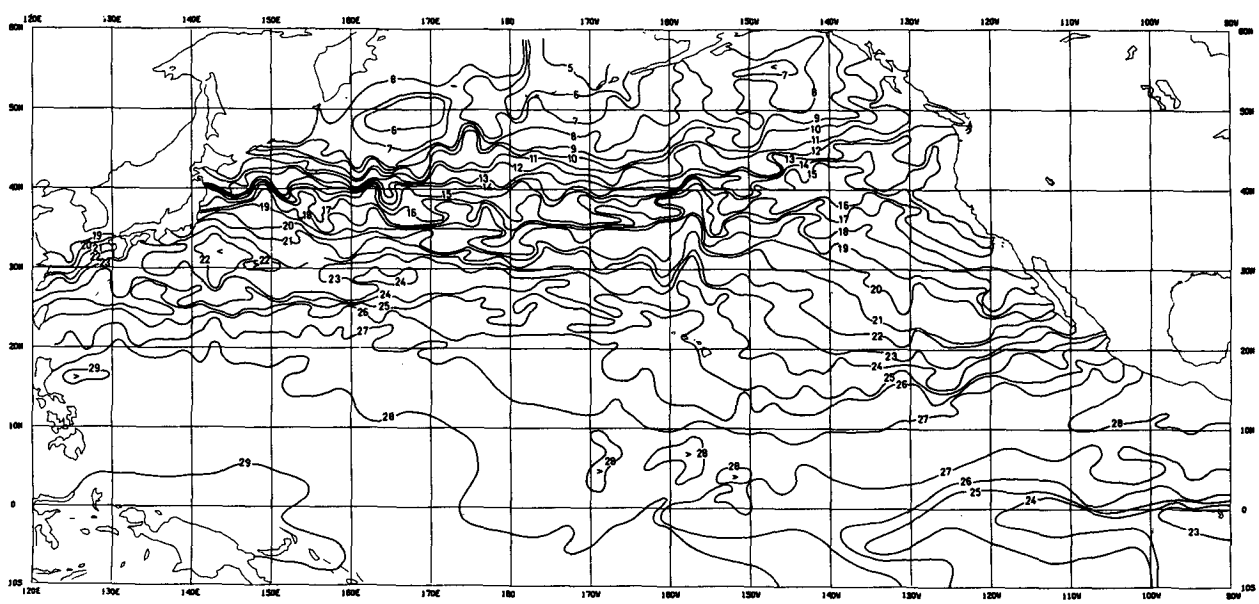

FIG. 7b. Mean annual sea surface temperature (°C)—North Pacific.

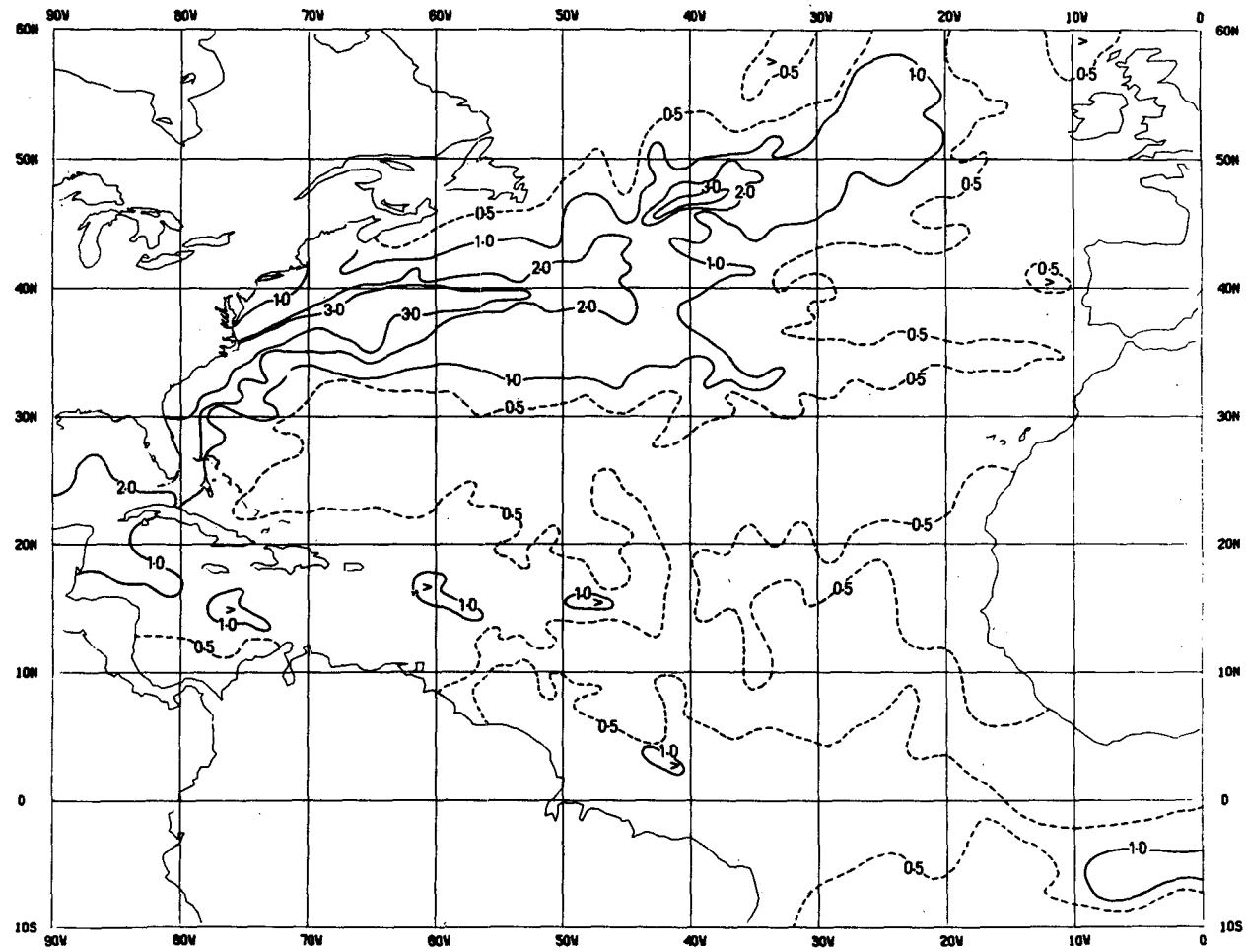

FIG. 8a. Temperature standard deviation (°C) at 400 m—North Atlantic.

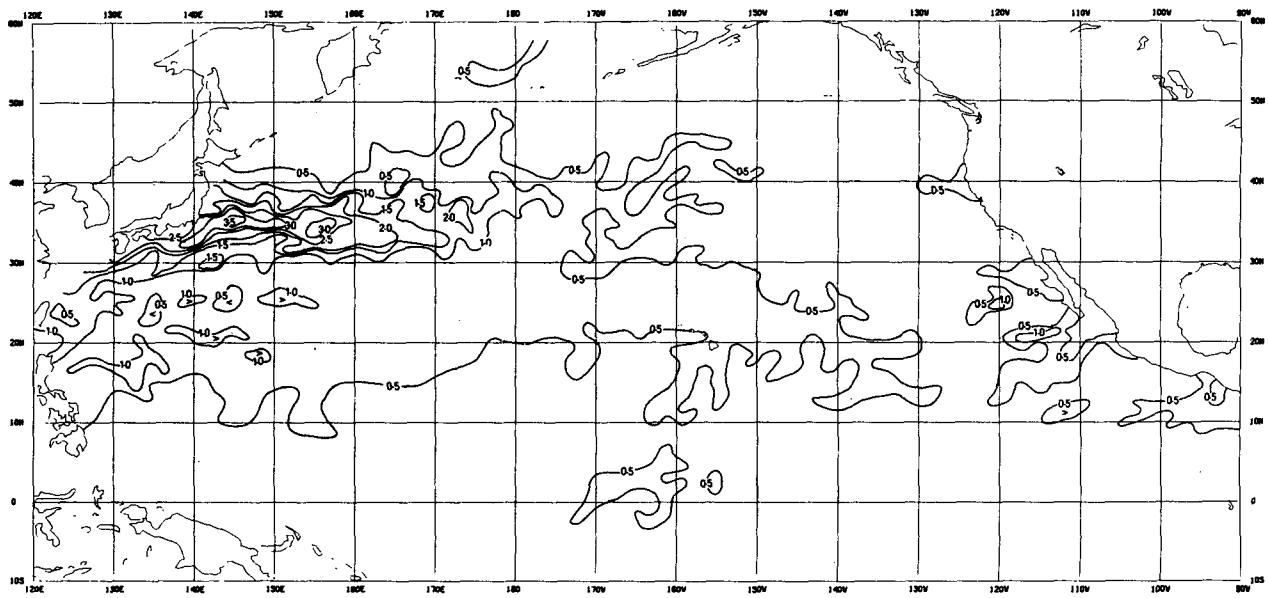

FIG. 8b. Temperature standard deviation (°C) at 400 m—North Pacific.

which exhibited lower rms differences (Emery and Dewar, 1982) for *TS* inferred dynamic height at almost all 5° square locations. Recent work by Stramma (1981) and Siedler and Stramma (1982) have confirmed the validity of using mean *TS* curves to compute dynamic height in the subtropical northeast Atlantic. They found that the method produces reliable dynamic heights not only for the 0 to 500 m layer but also for 0 to 1000 m.

As a check on the use of mean *TS* curves in the Pacific it was decided to use *TS* and *SZ* curves alone to compute North Pacific maps of 0/500 db inferred dynamic height from the variable grid XBT climatology. In addition a similar map was made using a combination of *TS* and *SZ* curves in the appropriate regions as defined by Emery and Dewar (1982). Failures of each method should stand out as clearly fictitious geostrophic current patterns in the inferred dynamic height maps. For the North Atlantic no combination of *TS* and *SZ* curves was used and only maps using mean *TS* curves were produced.

In Fig. 9a the 0/500 db *TS* inferred dynamic height map, for the North Atlantic, displays most of the general features found in published maps of the true dynamic height field. Northeast of Cape Hatteras the strong gradient is between 60 and 90 dyn cm in both Fig. 7a and the 100/700 db dynamic topography of Stommel *et al.* (1978, reproduced here as Fig. 10). This gradient in the latter map exhibits a greater number of smaller scale meanders than Fig. 9a, while the *TS* inferred topography contains an isolated maximum (anticyclonic circulation at 40°N, 58°W) associated with this gradient not present in Fig. 10. Both features reflect the known meandering of the Gulf Stream downstream of the Cape. The large maximum in Fig. 9a is not a strong feature in the 400 m temperature (Fig. 5a) appearing only as a slight northward deflection of the isotherms. Thus its existence is likely due to the influence of the mean *TS* curves which in this region (Emery and Dewar, 1982) have very large standard deviations in salinity. This increased salinity variability is due to the sporadic introduction of fresher Slope Water into the region.

Another important difference between Fig. 9a and the map of Stommel *et al.* (1978, herein Fig. 10) is the absence in Fig. 9a of a narrow ridge or maximum, paralleling the coastline, between 25 and 35°N. Higher values are instead found in a maximum south of Cuba. It is interesting to note that the westward tongue of warm water (along 35°N) seen in the 400 m temperature is reflected in Fig. 9a as a sharp geostrophic flow inflection. A similar circulation pattern, at this location, was suggested by Wüst (1935, Fig. 47) from the density at 200 m. This feature is missing in Fig. 10 from Stommel *et al.* (1978).

The suggested circulation pattern of the Antilles Current, south of Cuba, is in sharp contrast to the more traditional pattern in Wüst's map. The apparent closed circulation is likely due to changes in nearshore *TS* properties leading to artificially high *TS* inferred dynamic heights just south of Cuba.

Other general patterns, however, agree fairly well with the 70 dyn cm contour, for example, trending southeastward, in both maps, from 40°N, 45°W to the coast of northwest Africa at about 22°N. Likewise farther north the 40 dyn cm contour turns toward the north at about 42°N, 50°W and again toward the east at 50°N, 42°W in both maps. Agreement is poorest between 0 and 30°N where the maximum tongue, in Fig. 9a, is far south of the much broader maximum in the Stommel *et al.* (1978) map. It should be remembered that this earlier map is based on a limited number of hydrographic sections, collected over a wide span of time and can, therefore, be expected to differ from a map constructed using averages over a large sample of more recent data.

The apparently close relationship between subsurface temperature patterns, and those of upper layer dynamic topography can be easily seen by comparing Figs. 5a and 9a. A pattern correlation of 0.6 was computed between the temperature at 400 m and the inferred dynamic topography.

For latitudes south of 40°N, in the North Pacific, *TS* inferred dynamic height (Fig. 11a) has been found (Emery and Dewar, 1982) to be a fairly reliable estimator of upper layer dynamic height. As in the map of Wyrtki (1974, here included as Fig. 12) the strong gradient, off Japan, extends out to about 150°E where the contours begin to spread as they trend to the east. The 140 dyn cm contour turns sharply south at about 140°E in both maps while a similar southward turn in the 130 dyn cm line occurs east of 150°E. Outlining the main anticyclonic gyre the 130 dyn cm contour, in both maps, extends eastward along 25°N just past Hawaii where it turns south and then west to close the gyre. The ridge along 10°N is well marked in both maps as is the smaller ridge, farther east along the equator. The contours in Fig. 11a are generally more convoluted than those in Fig. 12 due to the greater spatial resolution in the variable grid map.

North of 40°N the abundance of narrow, zonal maxima and minima (Fig. 11a) indicates the region where the *TS* salinity inference breaks down. No such features can be seen in the traditional map in Fig. 12. By comparison the *SZ* inferred dynamic height (Fig. 11b) looks much more realistic in this high-latitude region. Here the 70 and 80 dyn cm contours agree quite well with those in Fig. 12. The agreement breaks down rapidly below 40°N where the *SZ* inferred topography (Fig. 11b) begins to show smaller scale features not present in either Figs. 11a or 12.

Following the suggestion in Emery and Dewar (1982) a combination of *TS* and *SZ* methods was used to compute the inferred dynamic topography in

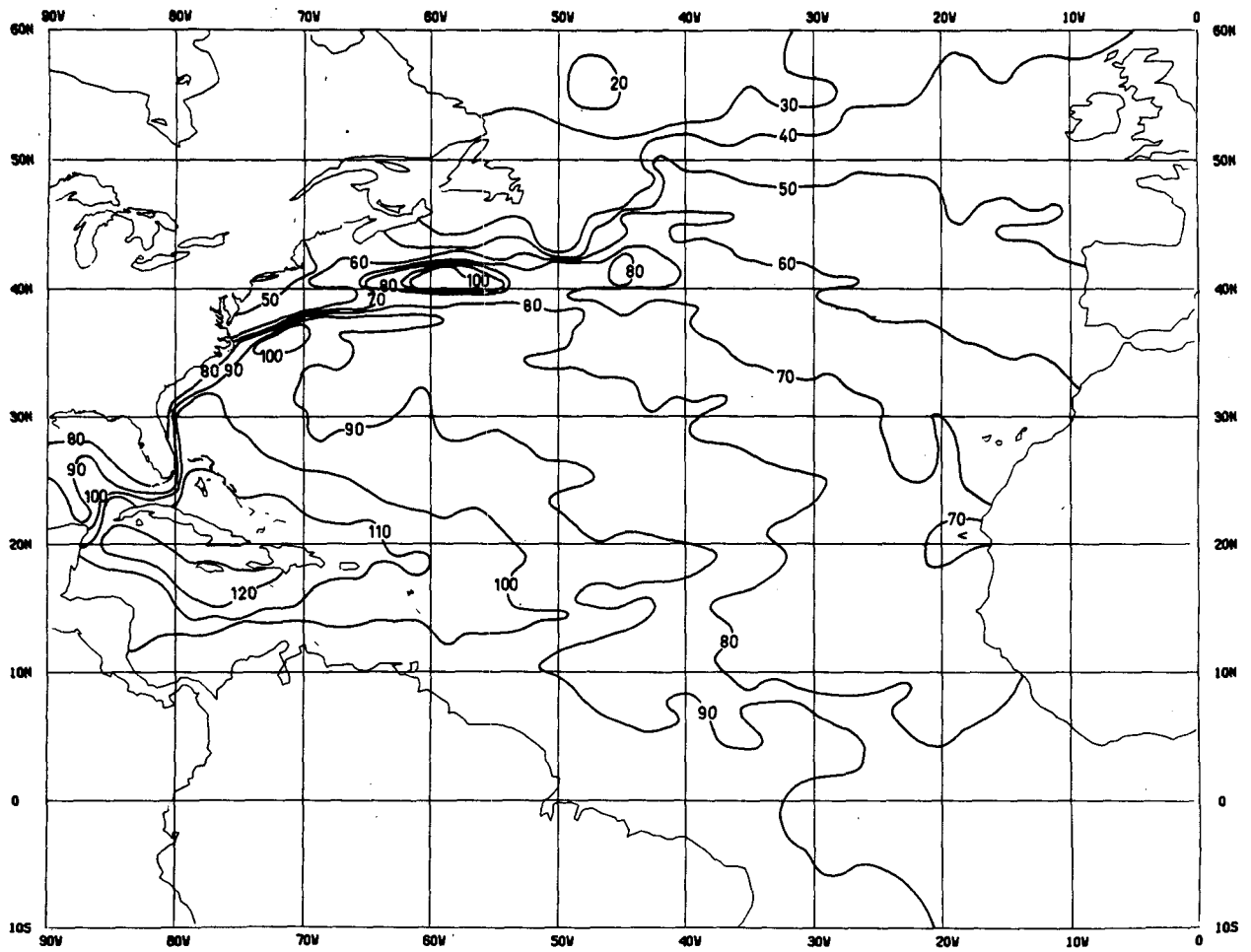

FIG. 9. 0/500 db *TS* inferred dynamic topography (dyn cm)—North Atlantic.

Fig. 11c. Generally the shift in methods occurred at 40°N but specific regions of *TS* or *SZ* application were defined by a comparison between true and inferred dynamic height carried out by Emery and Dewar (1982). The combined *TS*/*SZ* map (Fig. 11c) agrees very well with the dynamic height map (Fig. 12) produced by Wyrtki (1974). Except in the southwest the contours of Fig. 12 look like smoothed versions of those in Fig. 11c.

As with the Atlantic the 400 m temperature map (Fig. 5b) appears to reflect the inferred dynamic height patterns in Fig. 11c. Correlations were computed between the values in Fig. 11c and the temperature at 400 m for the eastern and western Pacific separately. East of the dateline the correlation is 0.81 while to the west it is even higher at 0.87.

6. The standard deviation of inferred dynamic height and eddy potential energy

Along with the mean inferred dynamic topography the XBT file was used to compute maps of the standard deviation, in 0/500 db inferred dynamic height. For the North Atlantic the general pattern (Fig. 13a) is again very similar to the eddy potential energy map of Dantzler (1977, herein Fig. 2). Highest values are in a ridge along 40°N extending out from North America. The core of this ridge appears to terminate between 50 and 60°W while the broader maximum continues eastward to between 30 and 40°W. The minimum, between 20 and 30°N, is much broader in the dynamic height deviation (Fig. 13a) than in the temperature deviation (Fig. 5a), in agreement with Danztler's map (Fig. 2). On the other hand the maximum in Fig. 13a, around 20°N, is much narrower and less continuous than the analogous features in Figs. 5a and 2.

The map of inferred dynamic height standard deviation for the Pacific (Fig. 13b) was computed using the combination of *TS* and *SZ* curves introduced earlier. Thus it should provide a good estimate of geostrophic current variability at all latitudes. Again there is a good correspondence between Fig. 13b and

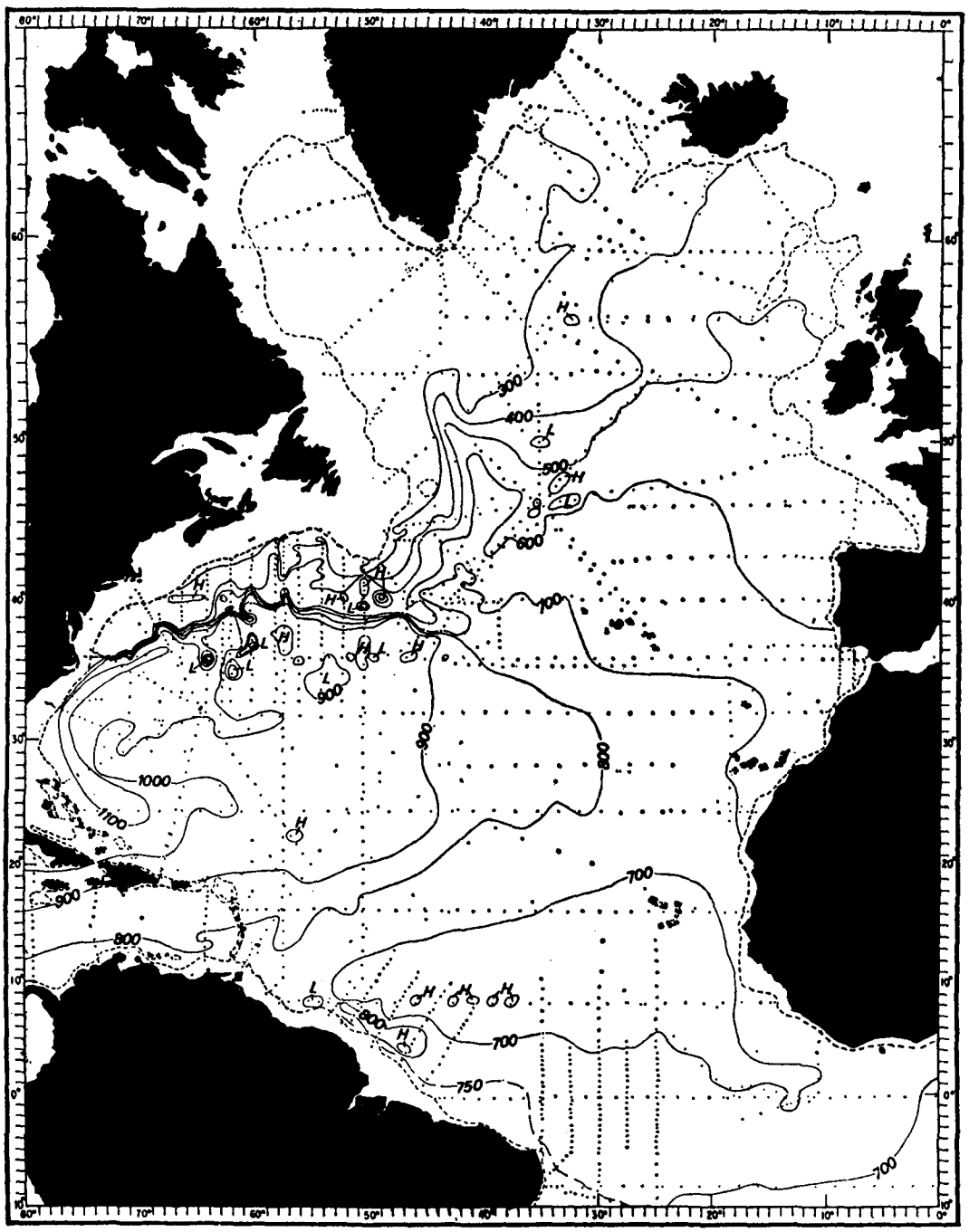

FIG. 10. Relative topography of 100 db relative to 700 db (dyn mm) from Stommel *et al.*, 1978).

the 400 m temperature deviations in Fig. 5b. Both have a tongue of high values running east from Japan along 35°N which terminates at about the dateline. It may be that the limit of the eastward tongue is related to the interaction with the Emperor Seamounts at this longitude as suggested by Bernstein and White (1977).

In his review of Pacific dynamic topography Wyrtki (1974) also produced a limited map of the standard deviation in 0/500 db dynamic height. In the data populous region off Japan he shows a maximum > 20 dyn cm stretching out to about 160°E. In Fig. 13b the core of the maximum is above 30 dyn cm while the 20 dyn cm contour does extend just past

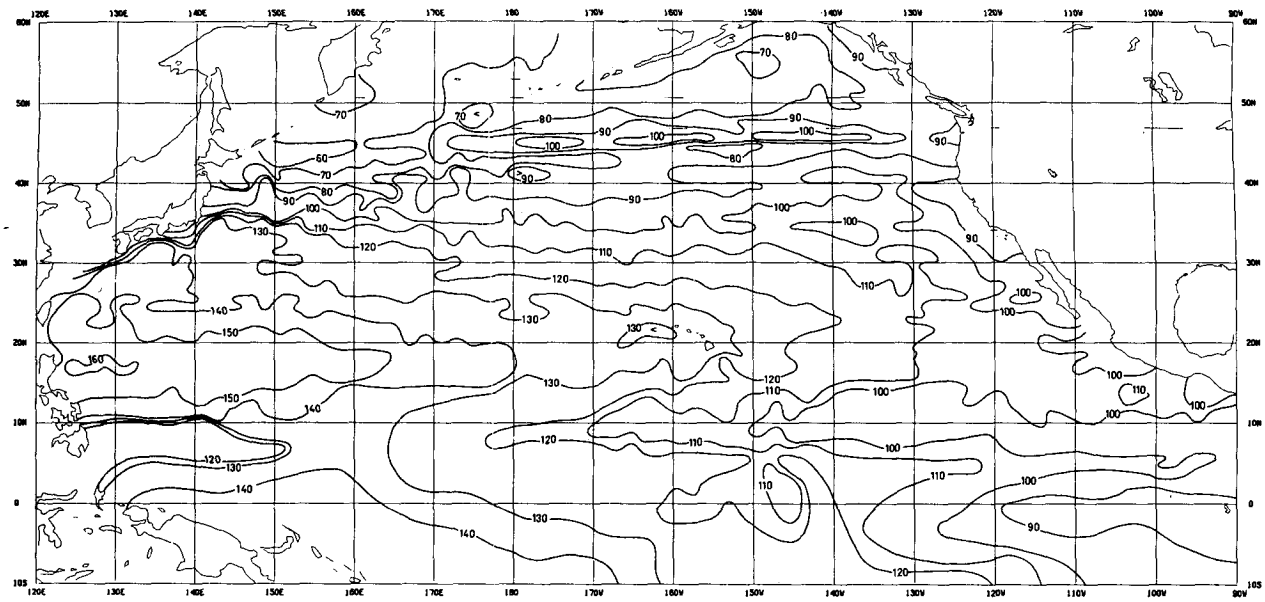

FIG. 11a. 0/500 db *TS* inferred dynamic topography (dyn cm)—North Pacific.

160°E. South of 30°N and west of 170°E Wyrtki's map indicates deviations less than 10 dyn cm while those in Fig. 13b are generally between 10 and 15 dyn cm. Both presentations show a decrease in amplitude at the longitude of Hawaii but the pertinent contour is 10 dyn cm in Fig. 13b while it is 6 dyn cm in Wyrtki's map. Values in the eastern North Pacific are generally below 5 dyn cm in both maps.

The temperature standard deviations, computed as part of the variable grid XBT climatology, can be used to estimate eddy potential energy. Following Dantzler (1977) we can write the potential energy per unit mass as

$$\mathrm{PE} = \tfrac{1}{2}\overline{N^2}\zeta^2, \qquad (1)$$

where $\bar{N}$ is the depth-averaged Brünt-Väisälä Fre-

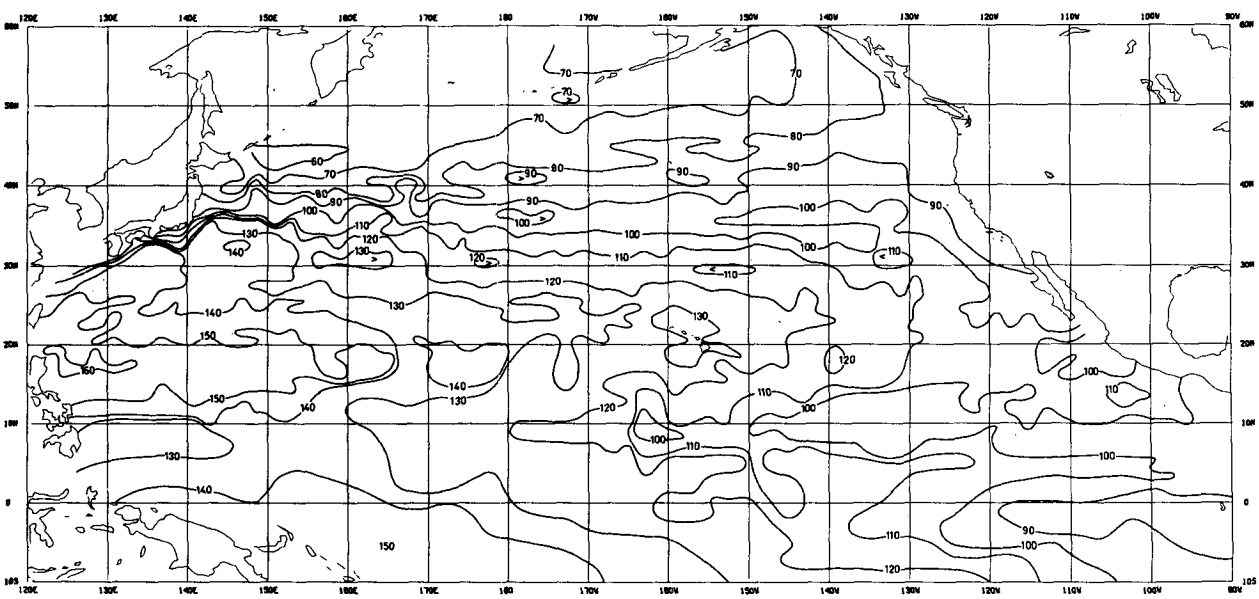

FIG. 11b. 0/500 db *SZ* inferred dynamic topography (dyn cm)—North Pacific.

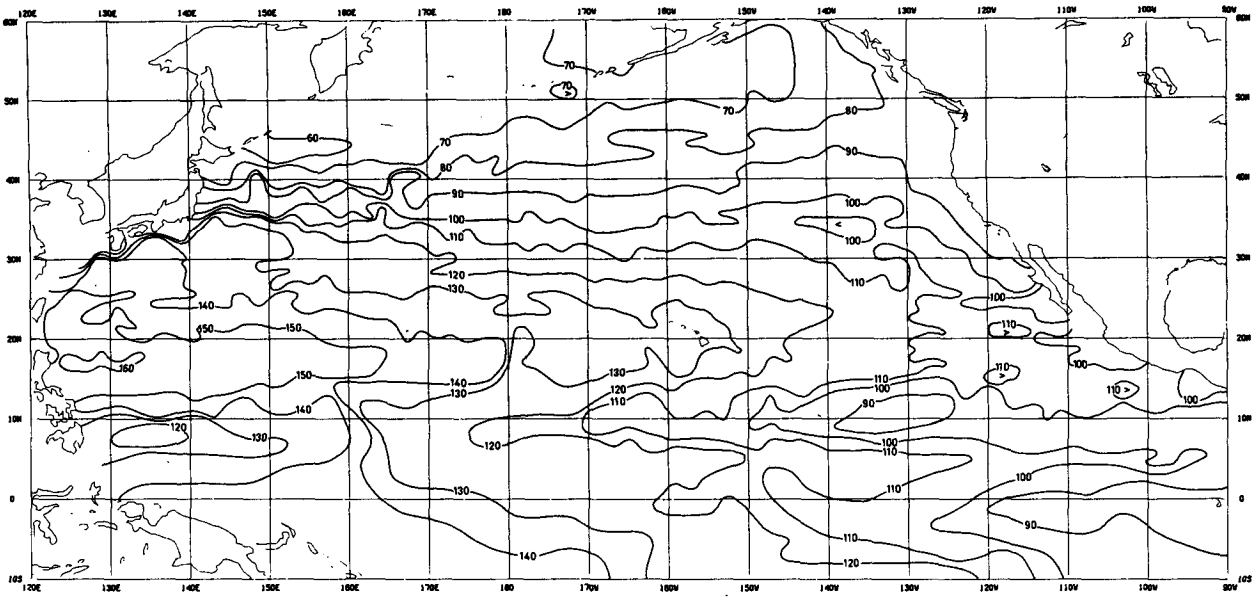

FIG. 11c. 0/500 db *TS-SZ* combined inferred dynamic topography (dyn cm)—North Pacific.

quency and ζ^2 represents the rms displacement of a chosen isotherm. Since

$$\overline{N^2} = \overline{\frac{g}{\rho}\frac{\partial \rho}{\partial z}} \tag{2}$$

and

$$\sigma_t = (\rho - 1) \times 10^3, \tag{3}$$

where ρ is density and z depth, we can write the potential energy as

$$\mathrm{PE} = \frac{1}{2}\frac{g}{\rho}\frac{\partial \sigma_t}{\partial z}\, 10^{-3}\zeta^2. \tag{4}$$

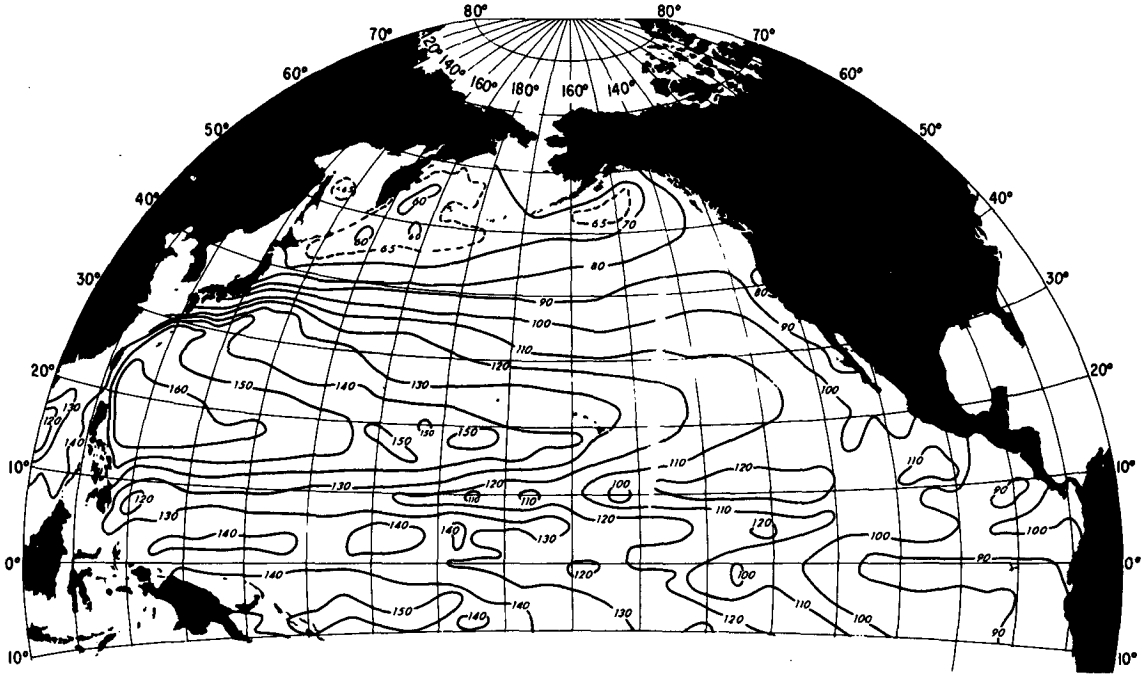

FIG. 12. Mean annual dynamic topography (dyn cm) of the sea surface relative to 500 db (from Wyrtki, 1974).

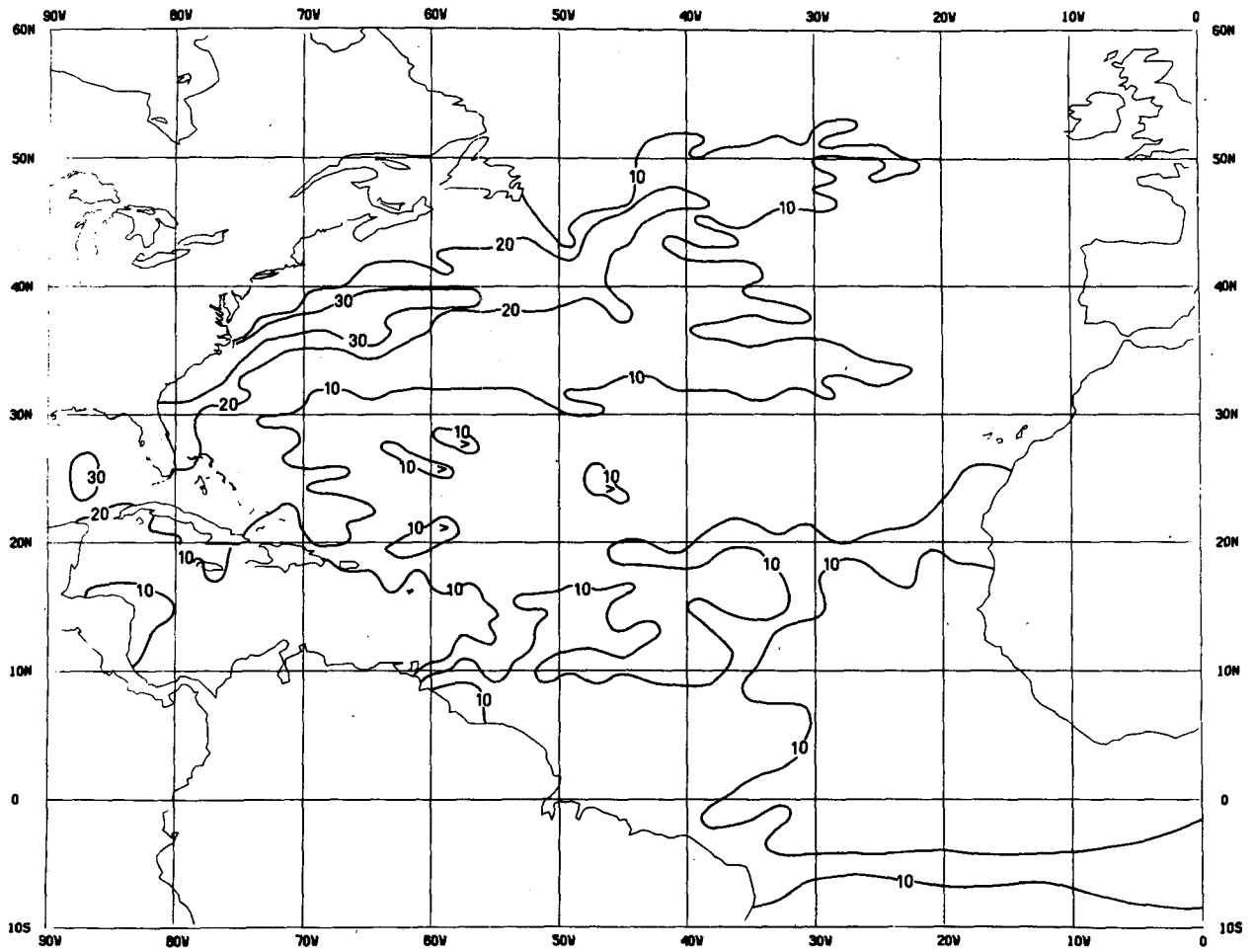

FIG. 13a. Standard deviation (dyn cm) in *TS* inferred dynamic height—North Atlantic.

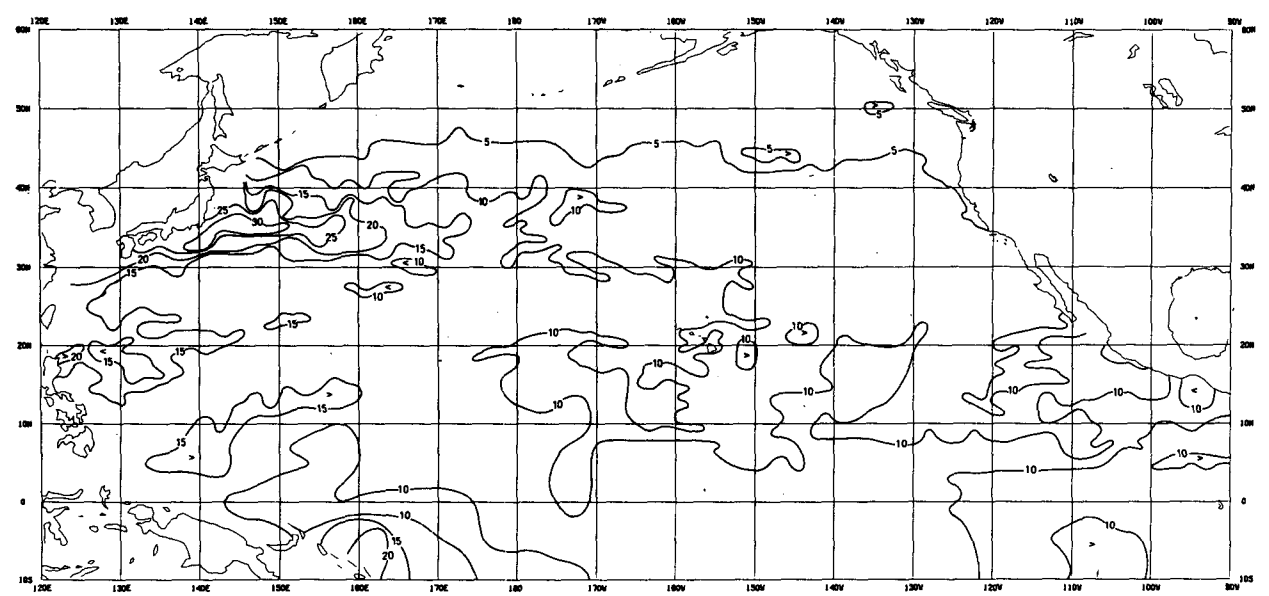

FIG. 13b. Standard deviation (dyn cm) in *TS–SZ* inferred dynamic height—North Pacific.

The assumption that vertical density gradients are well represented by gradients of σ_t is justified in the upper layer (<500 m) of interest where pressure effects are small. Rather than isotherm displacements, however, what we have computed are the standard deviations of temperature at certain depths along with the mean temperature profiles. Assuming that local vertical temperature gradients dominate we can utilize the familiar procedure of writing the isotherm displacements as

$$\zeta = \frac{T}{(\partial \bar{T}/\partial z)}. \tag{5}$$

Since we are interested in the rms isotherm displacements we can replace T by the temperature standard deviation (TSD). Thus we can write (4) as

$$\mathrm{PE} = \frac{1}{2}\frac{g}{\rho}\frac{\partial \sigma_t}{\partial z}\, 10^{-3}\left(\frac{\mathrm{TSD}}{\partial \bar{T}/\partial z}\right)^2, \tag{6}$$

where $\partial \bar{T}/\partial z$ can be taken from the XBT climatological mean temperature profiles. Converting all depths to centimeters to match the units in Dantzler's (1977) map, this becomes

$$\mathrm{PE} = \frac{1}{2}\frac{g}{\rho}\frac{\partial \sigma_t}{\partial z}\, 10^{-1}\left(\frac{\mathrm{TSD}}{\partial \bar{T}/\partial z}\right)^2. \tag{7}$$

Here ρ is taken as 1 and σ_t is computed from the mean temperature and the corresponding salinity from the mean TS curve (or SZ curves in the northern North Pacific).

The map of North Atlantic eddy potential energies at 300 m (Fig. 14a), computed using Eq. (7), can be compared directly with that of Fig. 2. As with earlier comparisons the general trends are very similar with largest values in the northwest, a zonal minimum band between 20 and 30°N, and a smaller maximum band along 20°N. Maximum values in Fig. 14a appear significantly higher than those in the earlier map; however, Dantzler (personal communication) computed values as high as 3200 $\mathrm{cm^2 s^{-2}}$ in the core of the maximum. This maximum, in the new map, is much narrower and extends farther east and north. The mid-latitude minimum in Fig. 14a is somewhat narrower than those in Fig. 2 and bends southward, in the west, unlike its counterpart. Also the smaller maxima in the south of Dantzler's map are completely missing in Fig. 14a.

In the previous section the standard deviation of inferred dynamic height (Fig. 13a) was considered as an estimate of eddy activity. Thus the distribution in Fig. 13a should compare fairly well with that of eddy potential energy in Fig. 14a. The pattern correlation was 0.59, somewhat less than anticipated. It may be that the relatively low correlation is due to problems associated with computing EPE from Eq. (7). It may be that the inferred dynamic height deviations are better estimates of eddy activity. As will be discussed next this is certainly the case in the eastern North Pacific. It should be remembered that the dynamic height deviation is computed as the integral over 0 to 500 m and thus represents variability at all these depths. The eddy potential energy, however, is calculated at a single depth and depends strongly on the assumption that the vertical temperature gradient is strong.

There is unfortunately no existing map of eddy potential energy for the North Pacific available for comparison with the estimate for 300 m presented in Fig. 14b. As expected, maximum values are contained in a tongue extending eastward from Japan. Smaller maxima, within this tongue, emphasize the fact that much of the meander activity of the Kuroshio occurs downstream of its separation from the coast (Taft, 1972). Lower values, just west of these maxima, were not anticipated however.

The very high values in the Gulf of Alaska are an artifact of the computational method. Unlike the western Pacific, where the high values are driven by large temperature standard deviations (Fig. 5a), the high values in the northeast are due to a very small mean vertical temperature gradient. As can be seen in Fig. 5a temperature standard deviations (here at 400 m) are relatively low in the Gulf of Alaska. Thus this method of estimating eddy potential energy is invalid in this high-latitude region, where salinity dominates, and one must rely on the map of inferred dynamic height deviation as an estimate of eddy activity.

The distribution in the central, mid-latitude Pacific is also much more complex in Fig. 14b than in the dynamic height variability in Fig. 13b. It is unlikely that the small-scale patchiness, in eddy energy, represents actual spatial variations but rather are expressions of inadequacies in the data or the method. The small maxima off Baja, California (Fig. 14b) appear to correspond to maxima in TSD at 400 m (Fig. 5b). Thus these regions are probably locations of increased eddy activity. It is curious that these maxima are to the south of regions of known eddy intensity (Bernstein *et al.*, 1977).

Spatial correlations between eddy potential energy and the standard deviation of inferred dynamic height were computed for the eastern and western (as defined earlier) North Pacific separately. In the east the artificially high values of eddy energy in the Alaskan Gulf, not present in the dynamic height deviations, resulted in a very low correlation of 0.11. West of the dateline the correlation jumped to 0.68 confirming the dependence of the high eddy energy values on thermal variability.

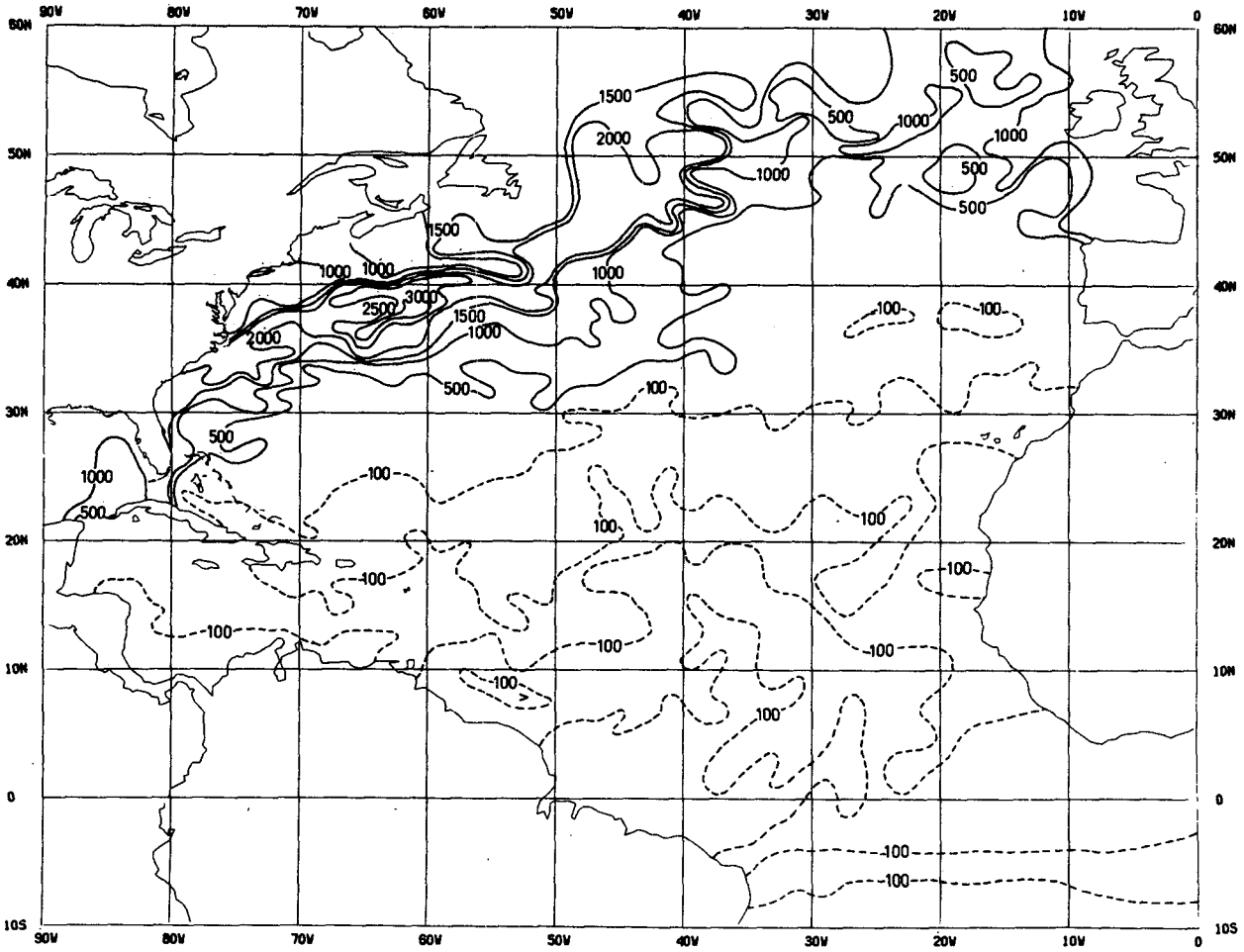

FIG. 14a. Eddy potential energy density ($cm^2\ s^{-2}$) at 300 m—North Atlantic.

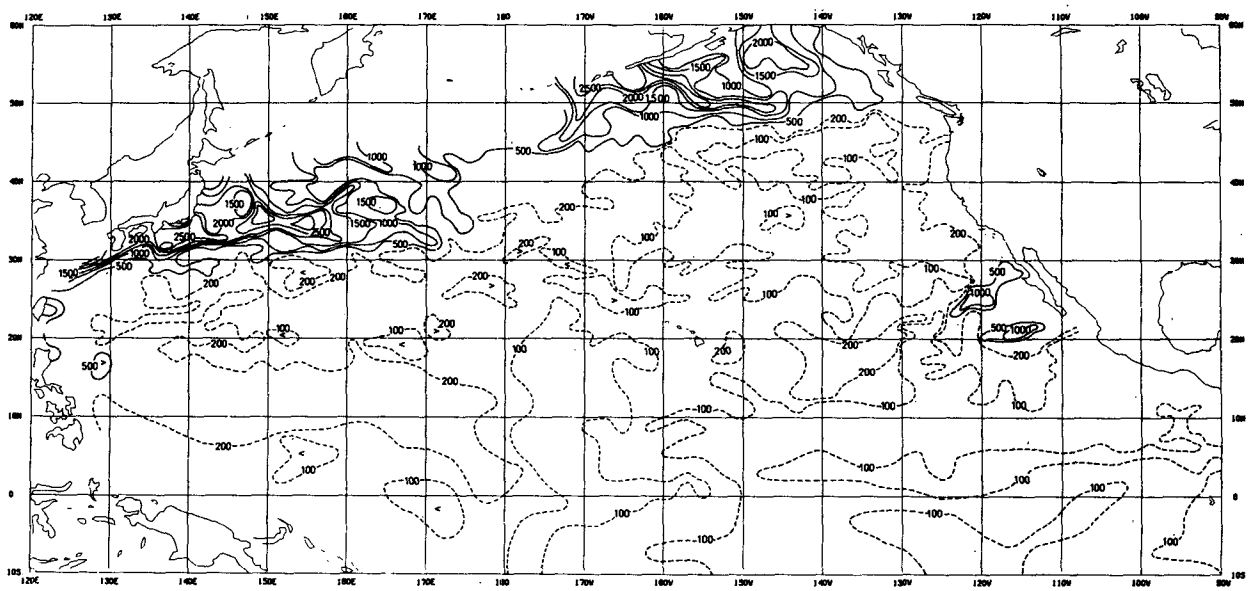

FIG. 14b. Eddy potential energy density ($cm^2\ s^{-2}$) at 300 m—North Pacific.

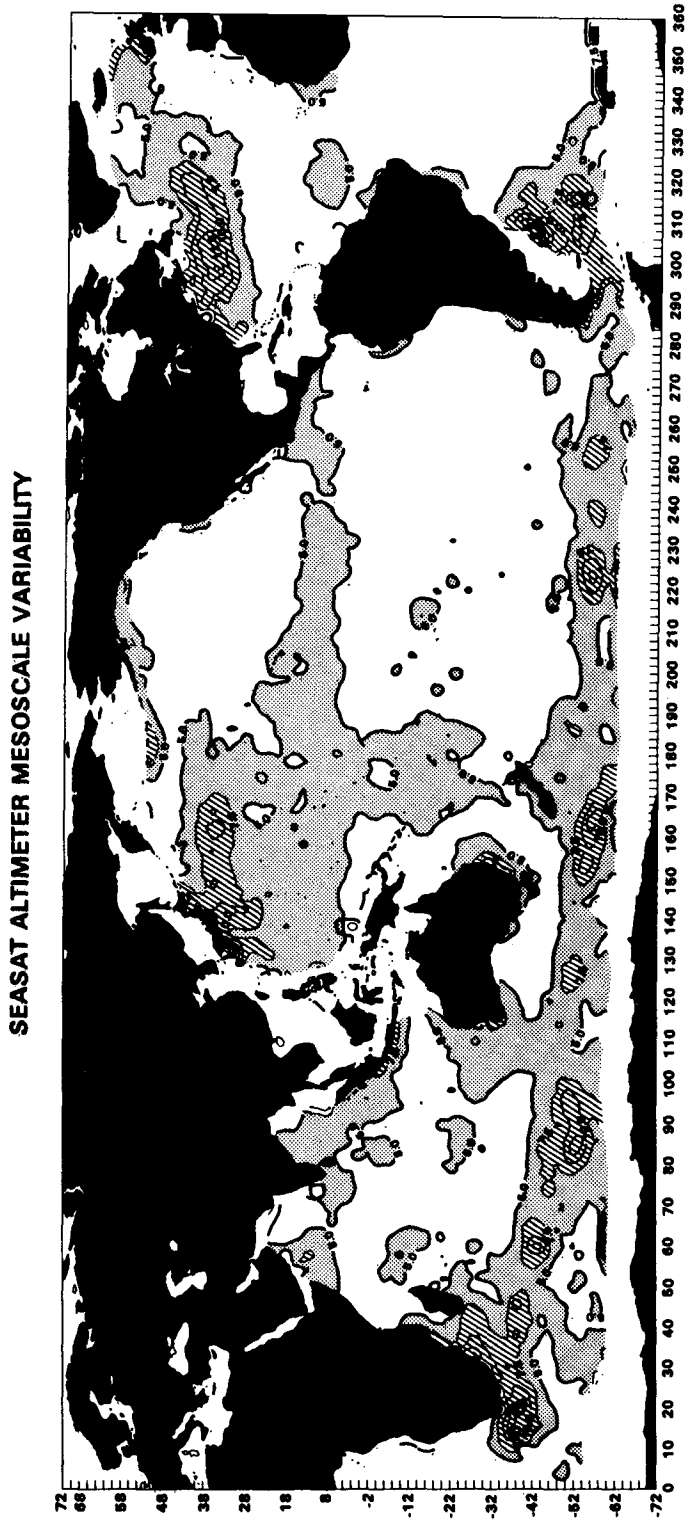

FIG. 15. Mesoscale variability from SEASAT altimetry (cm) from Cheney and Marsh (1981).

7. Comparison with SEASAT altimetry

A recent statistical analysis of SEASAT altimetry (Cheney *et al.*, 1981) has produced a global map of mesoscale variability (Fig. 15). These computations are based on repeated colinear tracks of the satellite. Along-track resolution is 7 km while the spacing, between tracks, can be as large as 800 km.

Comparisons between this map and the other maps of eddy variability presented in this paper, yield some very interesting results. The tongue of high values (>7.5 cm) in the northwest Atlantic (Fig. 15) extends eastward of 40°W, considerably beyond the similar maximum in the EKE of Fig. 1 and also beyond the maximum in Dantzler's eddy potential energy (Fig. 2). By contrast the maxima in Figs. 8a, 13a and 14a all extend eastward to between 20 and 30°W.

The agreement between the altimetric variability in Fig. 15 and the standard deviation in North Pacific inferred dynamic height (Fig. 13b) is also very good. Both contain tongues of high values stretching eastward from Japan beyond 170°E. In contrast, the similar maximum in the EKE map (Fig. 1) extends only out to about 165°E and is less well developed than the analogous features in either Fig. 13b or Fig. 15. It should be noted here that the high equatorial values of Wyrtki's (1974) EKE (herein Fig. 1) are absent in the maps of inferred dynamic height deviation, EPE and altimetric variability. The relatively low values of eddy variability in the Gulf of Alaska, from the SEASAT data (Fig. 15), are consistent with the lowest values in inferred dynamic height deviation (Fig. 13b) located in the Alaskan Gulf. This deviates sharply from the eddy potential energy estimates in Fig. 14b which exhibit artificially high values in this region.

8. Discussion

There are many limitations to the type of analysis presented in this study. Whenever one works with historical data editing procedures are limited to general statistics and one cannot examine each data record individually. After applying a variable grid, used to improve spatial resolution, one is left with the question of how much of the added spatial resolution is real information and should be retained in contouring, or how much is due to noise and should be smoothed over. In this paper an effort was made to display those features which had some spatial coherence while smoothing over those based on only a single grid value.

The comparisons between the mean fields, computed in this study, and those previously published by other investigators, support the validity of the large-scale distributions. It is encouraging that the *TS*/*SZ* inferred dynamic height map corresponds, in the North Pacific, so well with the map of 0/500 db true dynamic height published earlier by Wyrtki (1974). Since both of the products are annual averages, over a number of different years, the isopleths can be expected to agree well in position. That they do so is clearly a verification of the utility of inferred dynamic height using both *TS* and *SZ* curves. The poorer agreement between inferred and true dynamic height in the Atlantic may be explained by the differences in formulation. The map from Stommel *et al.* (1978) did not average data together but rather used selected stations to produce 100/700 db dynamic height. Thus it is not surprising if there are differences between this map and that of mean annual average 0/500 db *TS* inferred dynamic height.

Differences between the two new estimates of mesoscale variability, resulting from this study, and previous estimates are harder to explain. The EPE calculation is compromised by its dependence on the vertical temperature gradient being strong. The standard deviations in inferred dynamic height do not suffer from this restriction and appear to agree well with the recent estimate of mesoscale variability from SEASAT altimetry for both the North Atlantic and North Pacific. Thus the goal of producing, from the XBT file, a map of mesoscale variability in the North Pacific, consistent with one in the North Atlantic, has been achieved.

Acknowledgments. The author would like to thank the many people who contributed to the completion of this project. Tom Nicol carried out the initial computations from the XBT file and formulated the variable grid scheme. Denis Laplante developed programs to produce the many plots and computed the correlations. Maureen Douglas drafted the maps and Pat Lust typed the manuscript. The author would like to recognize the role of H. Lee Dantzler in inspiring the work and carefully reviewing the original manuscript.

Thanks go also to Bob Cheney for supplying the map of SEASAT altimetry and to two reviewers for valuable suggestions. This work was supported by the U.S. Naval Ocean Research Development Agency (NORDA) Ocean Measurements Program (OMP) under Grant N00014-81-G-0008. The author gratefully acknowledges this support.

REFERENCES

Bernstein, R. L., L. Breaker and R. Whritner, 1977: California current eddy formation: ship, air and satellite results. *Science*, **195**, 353–359.

——, and W. B. White, 1977: Zonal variability in the distribution of eddy energy in the mid-latitude North Pacific Ocean. *J. Phys. Oceanogr.*, **7**, 123–126.

Cheney, R. E., J. G. Marsh and V. Grano, 1981: Global mesoscale variability from SEASAT collinear altimeter data. *Trans. Amer. Geophys. Union*, **62**, p. 12 (abstract).

Dantzler, H. L., Jr., 1977: Potential energy maxima in the tropical and subtropical North Atlantic. *J. Phys. Oceanogr.*, **7**, 512–519.

Defant, A., 1936: *Wissenschaftliche Ergebnisse der Deutschen Atlantischen Expedition*, Vol. 6, *Atlas*. Verlag Von Walter de Gruyter & Co.

Dorman, C. E., and J. F. T. Saur, 1978: Temperature anomalies between San Francisco and Honolulu, 1966–1974 gridded by an objective analysis. *J. Phys. Oceanogr.*, **8**, 247–257.

Emery, W. J., 1975: Dynamic height from temperature profiles. *J. Phys. Oceanogr.*, **5**, 369–375.

——, and R. T. Wert, 1976: Mean *TS* curves in the Pacific and their application to dynamic height computations. *J. Phys. Oceanogr.*, **6**, 613–617.

——, and A. O'Brien, 1978: Inferring salinity from temperature or depth for dynamic height computations in the North Pacific. *Atmos. Ocean*, **16**, 348–366.

——, and J. S. Dewar, 1982: Mean temperature-salinity, salinity-depth and temperature-depth curves for the North Atlantic and the North Pacific. *Prog. Oceanogr.*, **11**, 219–305.

Robinson, M. K., 1976: *Atlas of North Pacific Ocean Monthly Mean Temperatures and Mean Salinities of the Surface Layer*. Dept. of the Navy, Washington, DC, Naval Oceanogr. Office, Ref. Publ. No. 2.

——, R. A. Bauer and E. H. Schroeder, 1979: *Atlas of North Atlantic–Indian Ocean Monthly Mean Temperatures and Mean Salinities of the Surface Layer*. Dept. of the Navy, Washington, DC, Naval Oceanogr. Office, Ref. Publ. No. 18.

Siedler, G., and L. Stramma, 1982: Dynamic height computations from Northeast Atlantic temperature data. (Submitted to *Oceanologia Acta*).

Stommel, H. S., 1947: Note on the use of the *T-S* correlation for dynamic height anomaly computations. *J. Mar. Res.*, **5**, 85–92.

——, P. P. Niiler and D. Anati, 1978: Dynamic topography and recirculation in the North Atlantic. *J. Mar. Res.*, **36**, 449–468.

Stramma, L., 1981: Die bestimung der dynamischen topographie aus temperaturdaten aus dem Nordostatlantik. Berichte Institut fuer Meereskunde Kiel, No. 84, 66 pp.

Taft, B. A., 1972: Characteristics of the flow of the Kuroshio south of Japan. *Kuroshio: Its Physical Aspects*, H. Stommel and K. Yoshida, Eds., University of Tokyo Press, 165–216.

White, W. B., and R. L. Bernstein, 1979: Design of an oceanographic network in the mid-latitude North Pacific. *J. Phys. Oceanogr.*, **9**, 592–606.

Wüst, G., 1935: *Schichtung und Zirkulation des Atlantischen Ozeans. Die Stratosphäre* [*The Stratosphere of the Atlantic Ocean*, W. J. Emery, Ed., 1978, Amerind, New Delhi, 112 pp.]

Wyrtki, K., 1974: The dynamic topography of the Pacific Ocean and its fluctuations. Rept. HIG-74-5 Hawaii Inst. Geophys., 19 pp.

——, L. Magaard and J. Hager, 1976: Eddy energy in the Oceans. *J. Geophys. Res.*, **81**, 2641–2646.